THE UNIVERSITY OF MICHIGAN

COLLEGE OF ENGINEERING
Department of Atmospheric and Oceanic Science

Technical Report

NUMERICAL EXPERIMENTS ON QUASI-GEOSTROPHIC TURBULENCE WITH CYCLIC BOUNDARY CONDITIONS

Vicente R. Barros[1)]

Aksel C. Wiin-Nielsen[2)]

DRDA Project 002630

[1)] Present affiliation: Servicio Meteorologico Nacional, Buenos Aires, Argentina

[2)] Present affiliation: European Centre for Medium-Range Weather Forecasts, Bracknell, U.K.

supported in part by:

NATIONAL SCIENCE FOUNDATION
GRANT NO. GA-16166
WASHINGTON, D.C.

administered through:

DIVISION OF RESEARCH DEVELOPMENT AND ADMINISTRATION ANN ARBOR

August 1974

TABLE OF CONTENTS

LIST OF ILLUSTRATIONS

LIST OF ILLUSTRATIONS (continued)

ABSTRACT

The results of various numerical experiments on quasi-geostrophic turbulence are presented and discussed. The model used for these experiments is essentially that described by Steinberg (1971, 1973).

The results presented are from four different experiments. In the first three of these the model was forced by maintaining a heat source at wave number 8. These experiments differed in the specifications of the frictional mechanisms which were used.

The fourth experiment contained the same frictional specification as the first one but the forcing was in wave number 1 (the largest permissible scale).

The discussion focusses predominantly on two features of the experiments. The first of these is the effect of varying the scale of the forcing on the approach to a quasi-steady energy spectrum. The second feature of interest is the effect of the frictional specification on the final shape of the energy spectrum, particularly as regards the slope of the spectrum for higher wave numbers.

In the later part of the report the distribution of energy under quasi-steady conditions is discussed theoretically for a specification of heating and frictional parameters typical of that used in experiment 3.

1. INTRODUCTION

In an earlier paper (Barros and Wiin-Nielsen (1974)), hereinafter referred to as BW the authors presented the results of a numerical turbulence simulation experiment using a two-level quasigeostrophic β-plane model. Although this experiment resembled that of Steinberg (1973) in some respects there were important differences, perhaps most significantly in the specification of lateral boundary conditions and the model forcing. The BW study used a β-plane channel and zonal velocity and thermal fields. The model was forced through diabatic heating via a Newtonian mechanism in which the equilibrium temperature field was a specified function of latitude. Although the purpose of the experiment reported upon in BW was to simulate large scale atmospheric flow it was also mentioned that a number of experiments had been carried out with the simplified model of Steinberg (1973). The purpose of these experiments was to examine the effects of changing various empirical parameters. We shall, in the present report, display and discuss some of the results of a selected group of these experiments, paying particular attention to the separate effects of changing the scale at which the model is forced and/or different specifications of frictional mechanisms.

2. THE MODEL

The model which was used is the quasi-geostrophic two level model as discussed in BW. The horizontal domain and boundary conditions which were used are as in Steinberg's (1973) study, i.e.

a square region with cyclic boundary conditions in both directions. Consistently with this the β-effect is neglected so that the governing equations for the model are then as follows:

$$\frac{\partial q_1}{\partial t} = -\vec{V}_1 \cdot \nabla q_1 + \frac{\lambda^2 R}{f_o c_p} H + \nu \nabla^2 q_1 - A(\zeta_1 - \zeta_3) \tag{2.1}$$

$$\frac{\partial q_3}{\partial t} = -\vec{V}_3 \cdot \nabla q_3 - \frac{\lambda^2 R}{f_o c_p} H + \nu \nabla^2 q_3 + A(\zeta_1 - \zeta_3) - K\zeta_4 \tag{2.2}$$

where the quantities and parameters entering into these equations are as explained in BW.

The square domain is divided into a grid of 64 points on each side such that $\Delta x = \Delta y = 475$ km. We follow the convention of Steinberg (1971) in defining a two dimensional Fourier expansion for a quantity such that

$$\psi = \sum_{\kappa=1}^{N} \psi_\kappa \tag{2.3}$$

where

$$\psi_\kappa = \sum_m \sum_n A_{m,n} e^{iJ(mx+ny)}, \qquad \max(|m|,|n|) = \kappa \tag{2.4}$$

and $J = 2\pi/L$ with $L = 64\Delta x$. The summation in 2.4 is over both positive and negative values of m and n with reality being ensured by requiring that $A_{-|m|,-|n|} = A^*_{|m|,|n|}$ where $()^*$ denotes the complex conjugate. Here N is the maximum of m or n allowed by the dimensions of the region and the grid length. In the present case N = 32.

The diabatic heating function, H, was specified by a first order Markov process as outlined by Steinberg (1973). In this process the heating fields at times t and t + Δt are related as follows

$$H^{t+\Delta t} = RH^{t} + [1 - R^2]^{1/2} \tilde{H}^{t+\Delta t} \qquad (2.5)$$

where $\tilde{H}$ is composed of Fourier components whose larger wave number is m_i. The amplitude of the Fourier coefficients are chosen randomly from a Gaussian distribution and normalized so as to maintain the total amplitude of $\tilde{H}$ at a specified constant value. The quantity m_i is specified and fixed for a given experiment.

In all experiments the time integration of the model was begun from an initial state of rest. In order to speed up the generation of available potential energy a value R = 0.8 was used for the first 100 time steps. Thereafter R was fixed at the value 0.7.

Finite differences were used to evaluate the right sides of 2.1 and 2.2, the Arakawa second order scheme being used for advective terms. The Adams-Bashforth scheme was used for time differencing.

Diagnostic calculations of the stream function fields at levels 1 and 3, the vertical motion field at level 2, and various energetics quantities were carried out every 24 time steps. For this purpose fast Fourier transforms were used to compute the Fourier coefficients of q_1 and q_3. The stream functions ψ_1 and ψ_3 are obtainable directly in transformed form from the definitions of q_1 and q_3:

$$\nabla^2\psi_1 - \lambda^2(\psi_1 - \psi_3) = q_1 \qquad (2.6)$$

$$\nabla^2\psi_3 + \lambda^2(\psi_1 - \psi_3) = q_3 \qquad (2.7)$$

These procedures are identical to those used by Steinberg (1973) and therefore need not be discussed further.

3. EXPERIMENTS

The relevant externally imposed parameters for the experiments which will be discussed here are presented in Table 1. We include also the number of time steps for each experiment in hours of simulated time. In each case the time step was one hour. All other parameters appearing in equations 2.1 and 2.2 were assigned the numerical values given in BW.

As illustrated in Table 1, experiments 1 and 4 differ only as to the wave number at which the forcing is applied, while experiments 2 and 3 are concerned with variations in the horizontal and Ekman frictional coefficients ν and k. The choice $m_i = 8$ was made to facilitate comparison with Steinberg's (1973) study. On the other hand it was found in BW that, although the forcing was in the lowest mode of the model (in that case the zonal thermal field) the major part of the potential to kinetic energy conversion took place in the baroclinically active part of the spectrum. To see if a similar behaviour could be obtained in the present model we chose also, in experiment 4, to force the thermal field in the lowest mode, in this case $m_i = 1$.

Table I

Externally imposed parameters and number of time steps for each experiment

Experiment No.	m_i	ν ($10^5 m^2 sec^{-1}$)	k ($10^{-6} sec^{-1}$)	A ($10^{-6} sec^{-1}$)	H ($10\ cm^2 sec^{-3}$)	Hours
1	8	0.0	4	0.5	77	1032
2	8	0.0	2	0.5	77	900
3	8	1.7	4	0.5	77	1008
4	1	0.0	4	0.5	77	1032

3.1 The Development of a Quasi-Steady Energy Spectrum.

The integration time for all experiments was long enough to ensure the development of a quasi-steady energy spectrum. This is illustrated, in Figure 3.1, for experiment number 1. In this case quasi-steadiness was reached after 200 time steps.

The approach to steadiness varies in an interesting way when the scale of the forcing is varied. This is illustrated in Figure 3.2 where similar results are presented for experiment 4. In this case there are several features which distinguish the time dependent behaviour from that illustrated for experiment 1. The presence of considerably more energy in experiment 4 indicates that the energy generation is more efficient in this case. It is also interesting to note that although available potential energy is initially predominant it is eventually exceeded by kinetic energy.

Another noteworthy feature is illustrated in the behaviour of the kinetic energy for wave numbers 1 and 4. While the kinetic energy in wave number 1 is predominant for several hundred time steps it is eventually exceeded by that in wave number 4. In fact, towards the end of the integration period the predominant amounts of both available and kinetic energy were to be found in wave numbers 3 to 5.

To illustrate the energetics of experiment 4 we show, in Figures 3.3 and 3.4 the non-linear cascades of available potential

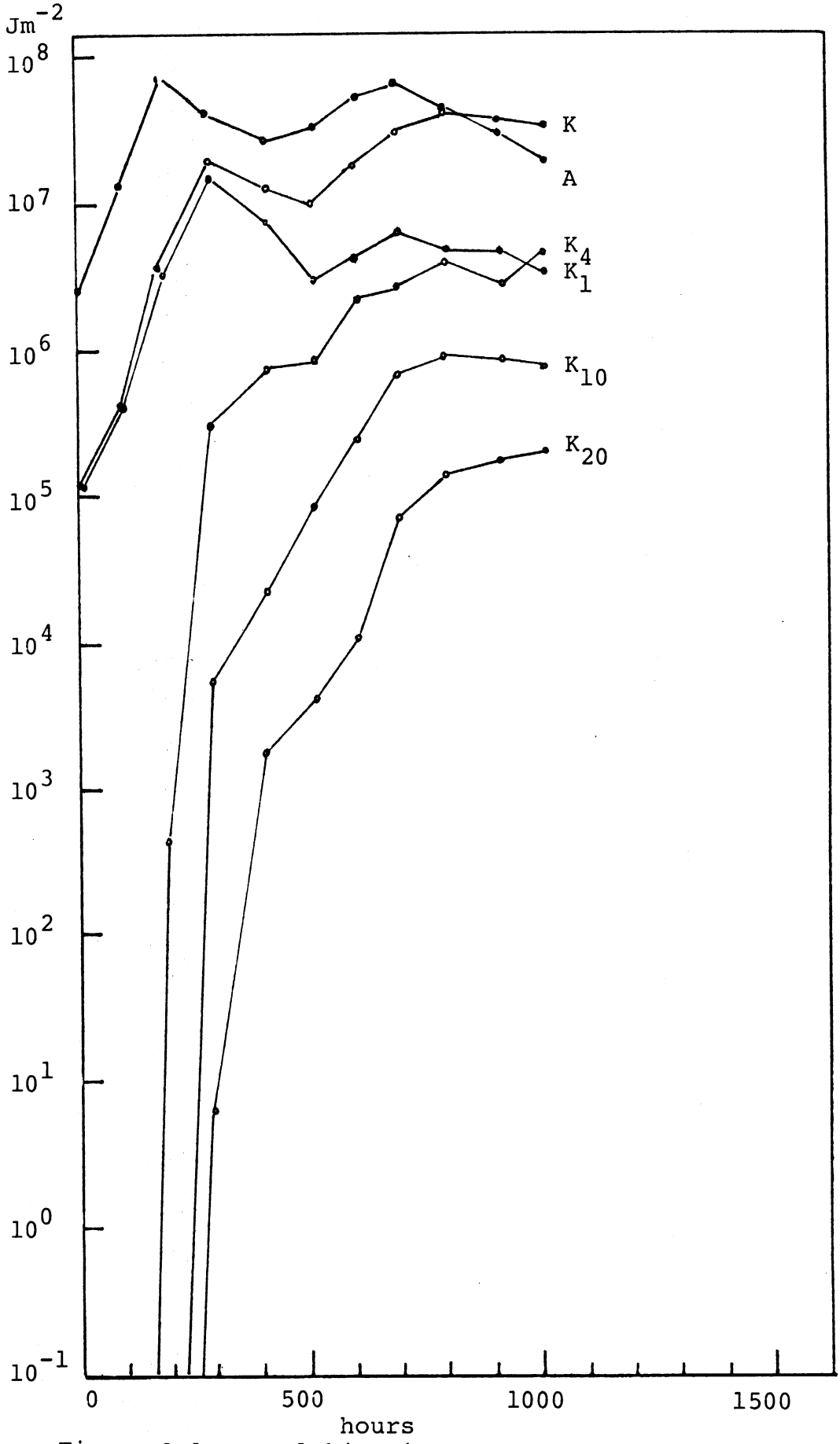

Figure 3.1: Total kinetic energy, total available potential energy and kinetic energy for wave numbers 1, 4,10 and 20 as a function of time.Units:Jm^{-2}.Exp.1.

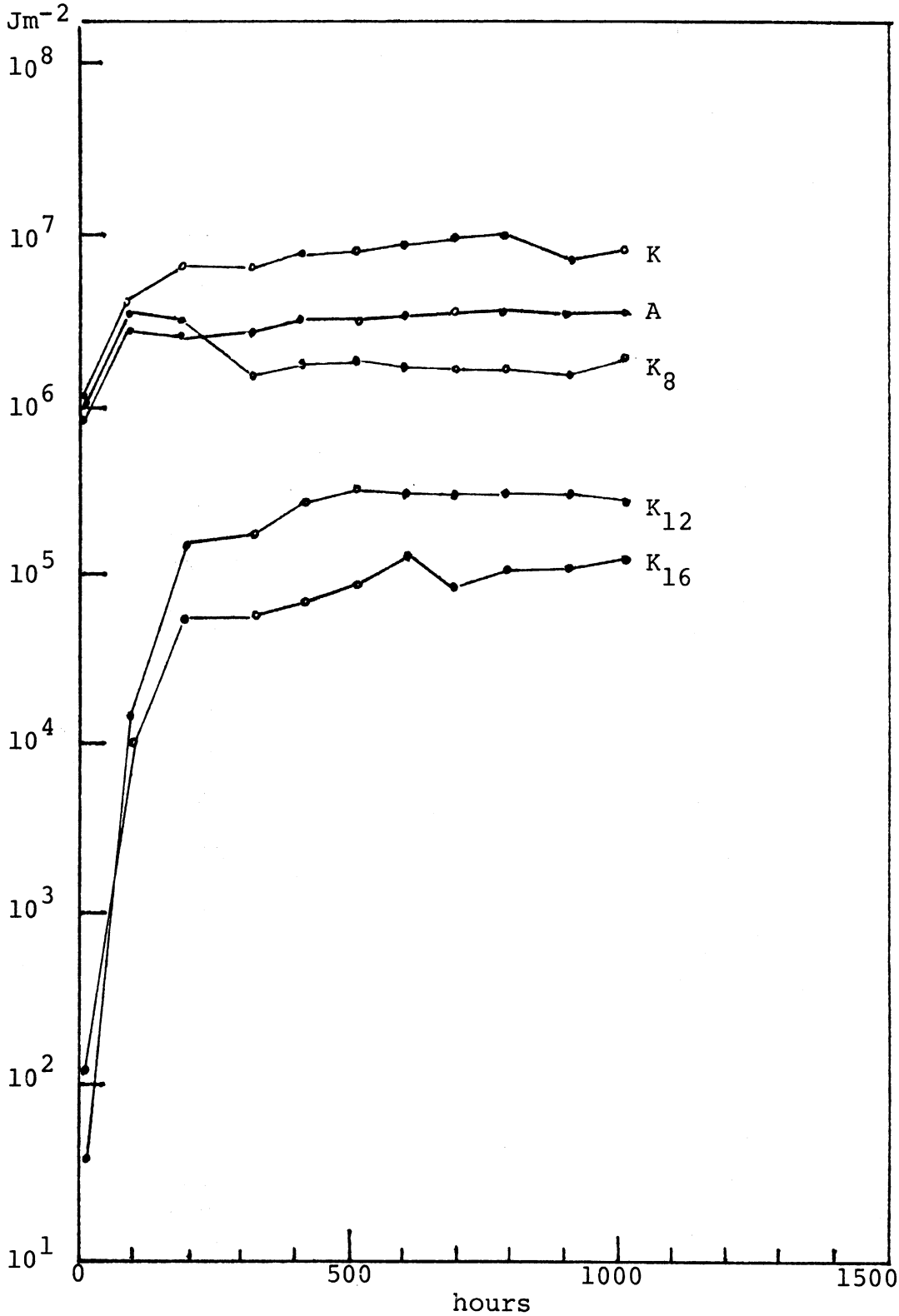

Figure 3.2: As Fig.3.1 but for wave numbers 8,12 and 16. Exp.4.

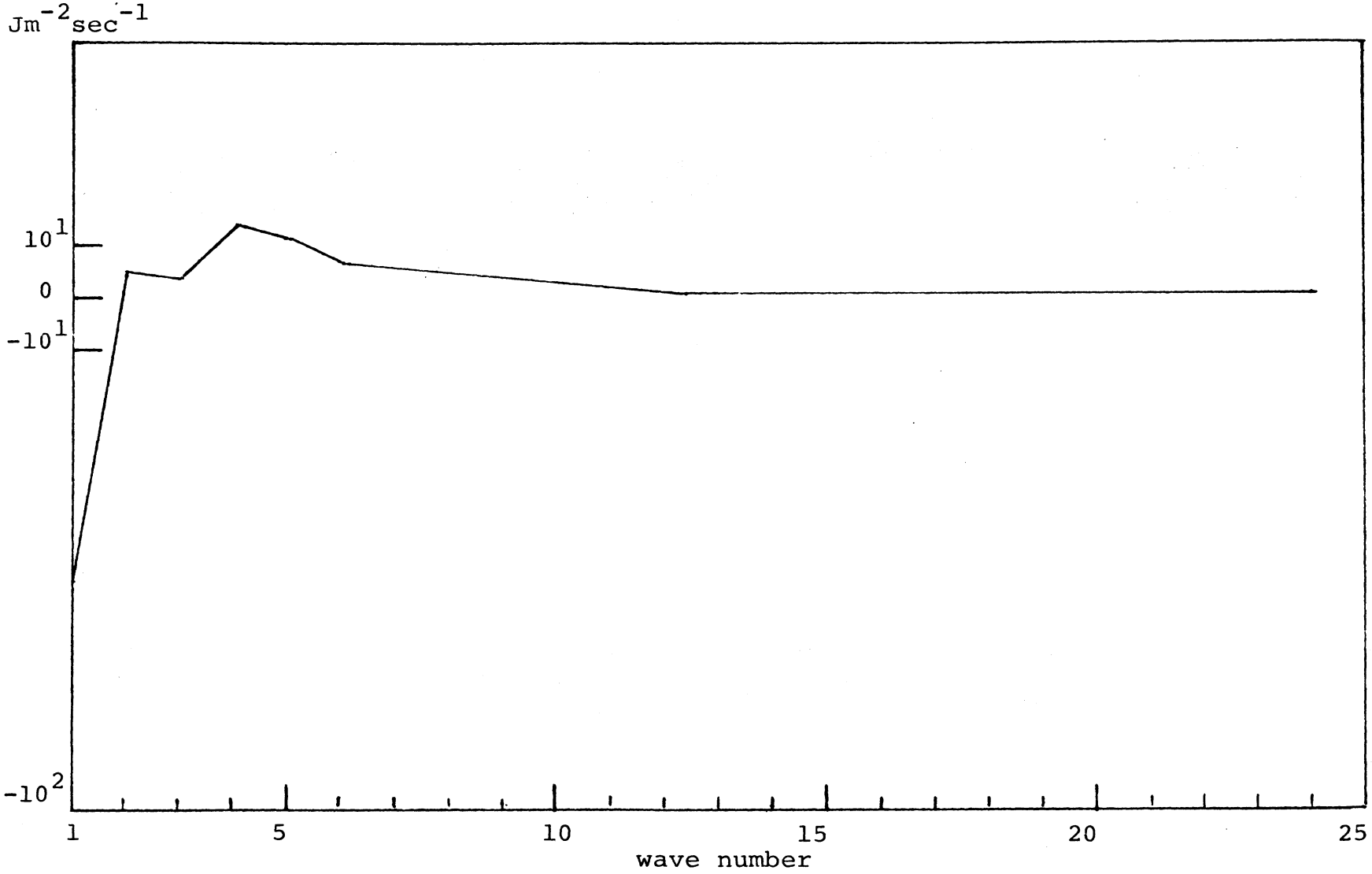

Figure 3.3: $C_A(m/n,\ell)$, nonlinear gain of available potential energy as a function of wave number. Units: J $m^{-2}sec^{-1}$. Exp.4.

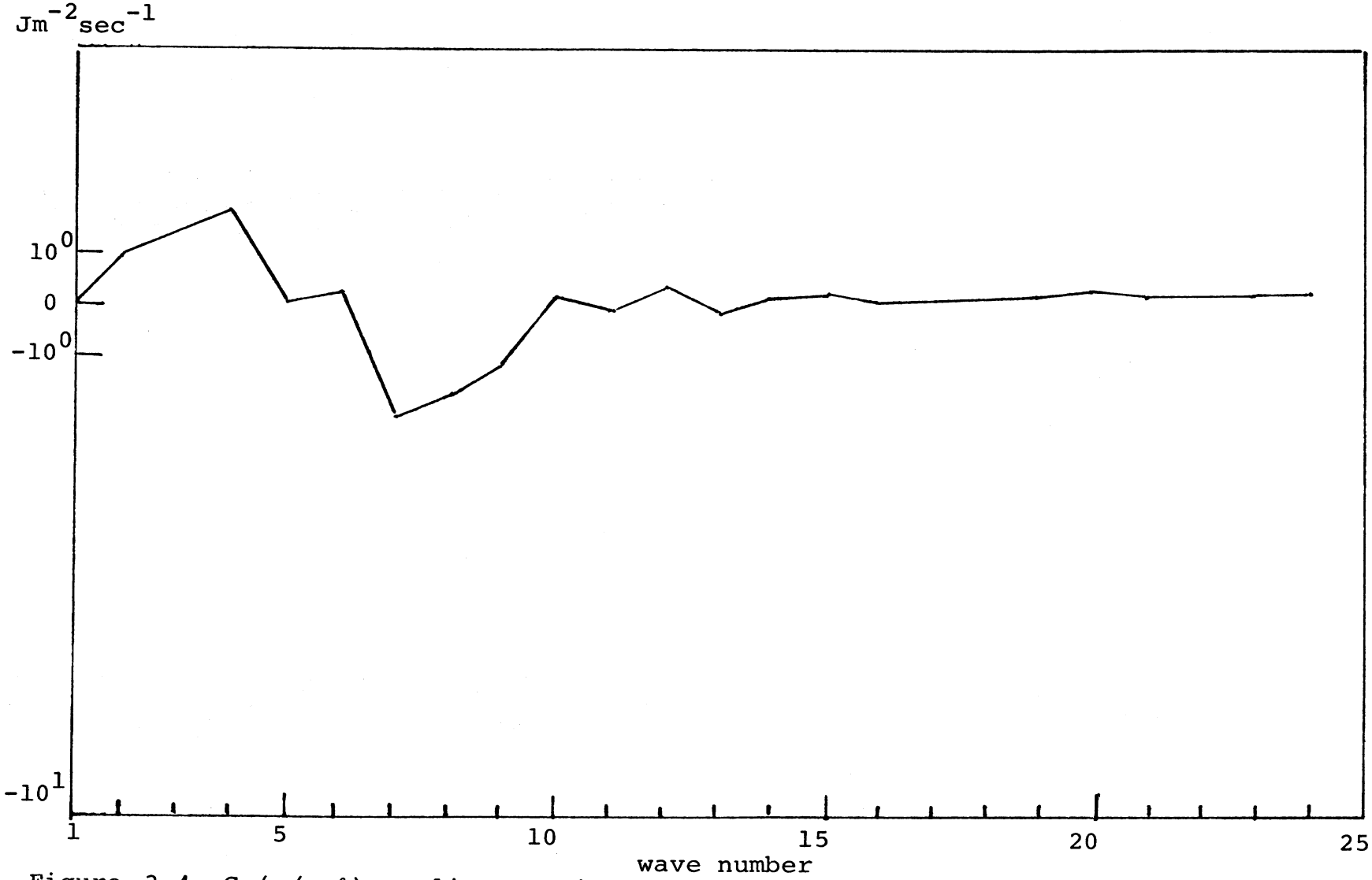

Figure 3.4: $C_K(m/n,\ell)$, nonlinear gain of kinetic energy as a function of wave number. Units: J m^{-2} sec^{-1}. Exp.4.

energy and kinetic energy. As illustrated by Figure 3.3, potential energy is cascaded to higher wave numbers with the dominant gain through non-linear interactions being in wave number 4. On the other hand Figure 3.4 shows that wave numbers 7 to 9 lose kinetic energy by the non-linear cascade process. Most of this cascade is to the larger scales ($2 \leq \kappa \leq 6$).

Figure 3.5 depicts the conversions of available potential energy to kinetic energy. Again, the dominant conversions are in the wave number range $3 < \kappa < 5$. Note that the quantity plotted in Figure 3.5 is C(K,A), and that $C(K,A) \leq 0$ for all wave numbers.

The kinetic energy, available potential energy, and enstrophy spectra for case 4 are shown in Figures 3.6 through 3.8 respectively. The slope of the kinetic energy spectrum in the range $10 < \kappa < 20$ is -2.2, somewhat less negative than the values which, as we shall illustrate below, were found for the remaining three experiments. The corresponding potential energy slope is consistent with what would be expected from the analysis of Merilees and Warn (1972).

Finally, we complete the documentation of case 4 by displaying, in Figure 3.9, the flux of enstrophy through the wave number domain. The procedure for computing this quantity has been outlined in BW. We note that, although the enstrophy flux is not constant anywhere, it varies by a relatively small amount in the range $9 < \kappa < 15$.

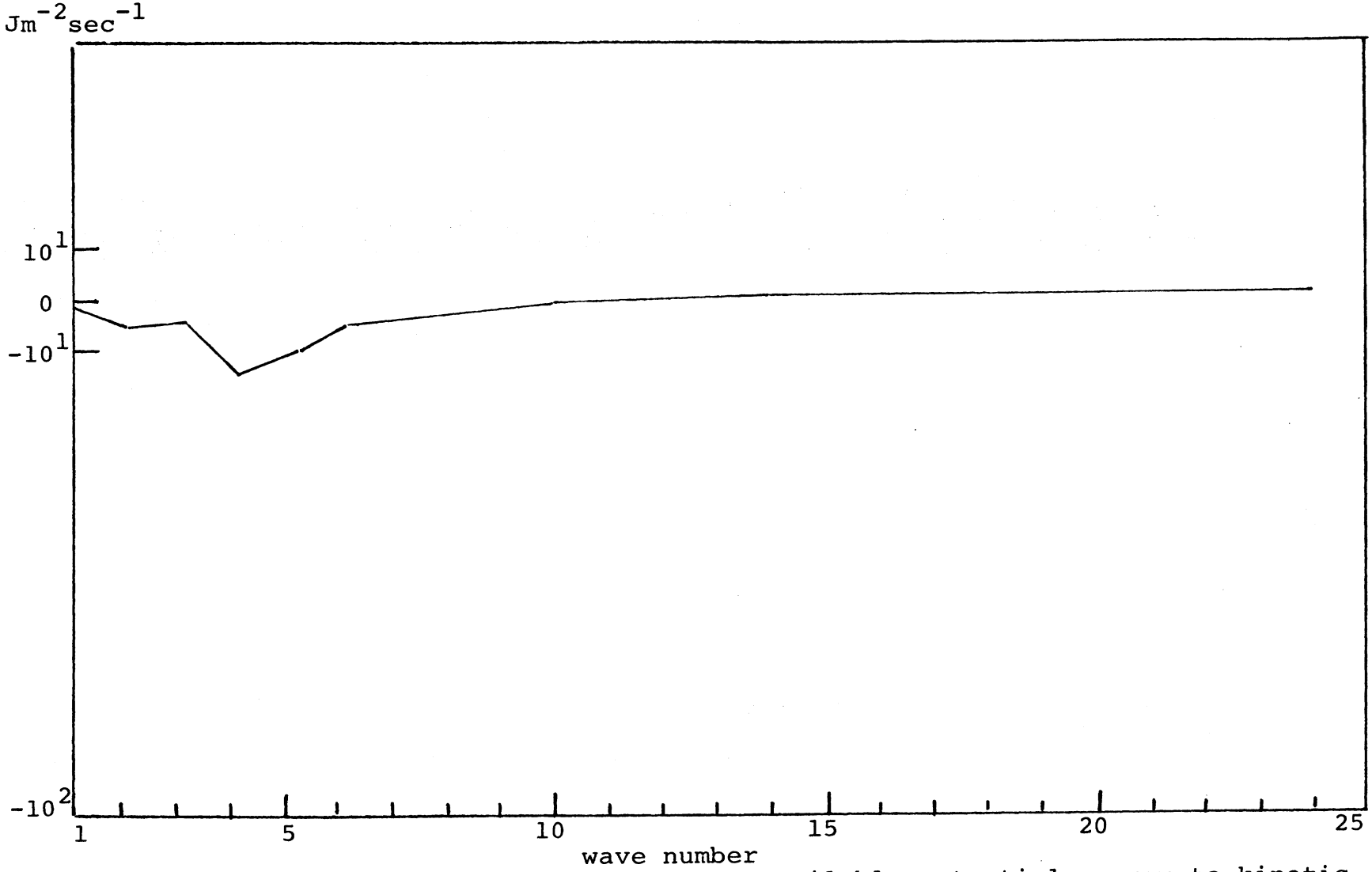

Figure 3.5: $-C(A_m,K_m)$, minus conversion from available potential energy to kinetic energy as a function of wave number. Units: $Jm^{-2}sec^{-1}$. Exp. 4.

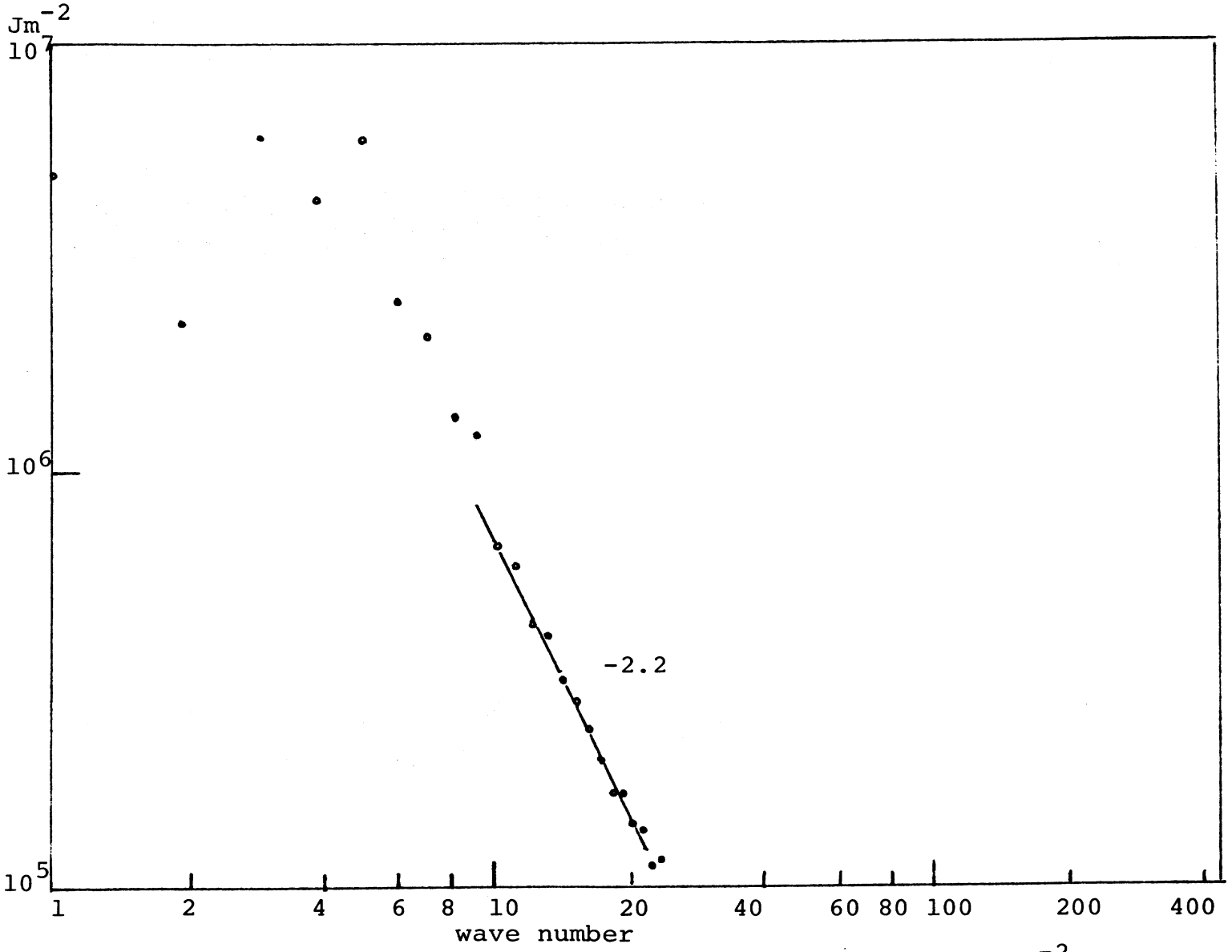

Figure 3.6: Kinetic energy as a function of wave number. Units: Jm^{-2}. Exp. 4.

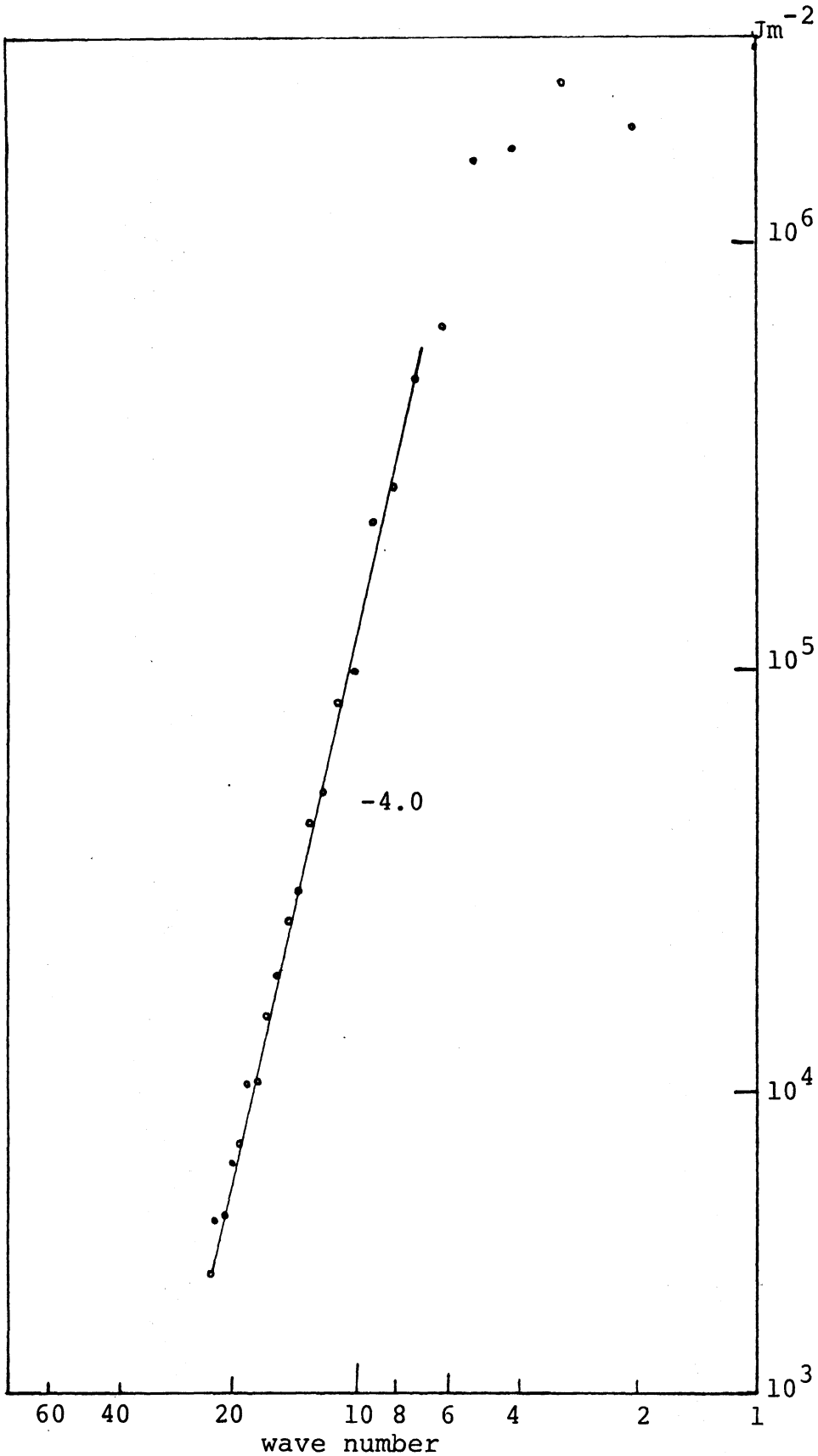

Figure 3.7: Available potential energy as a function of wave number. Units: Jm^{-2}. Exp. 4.

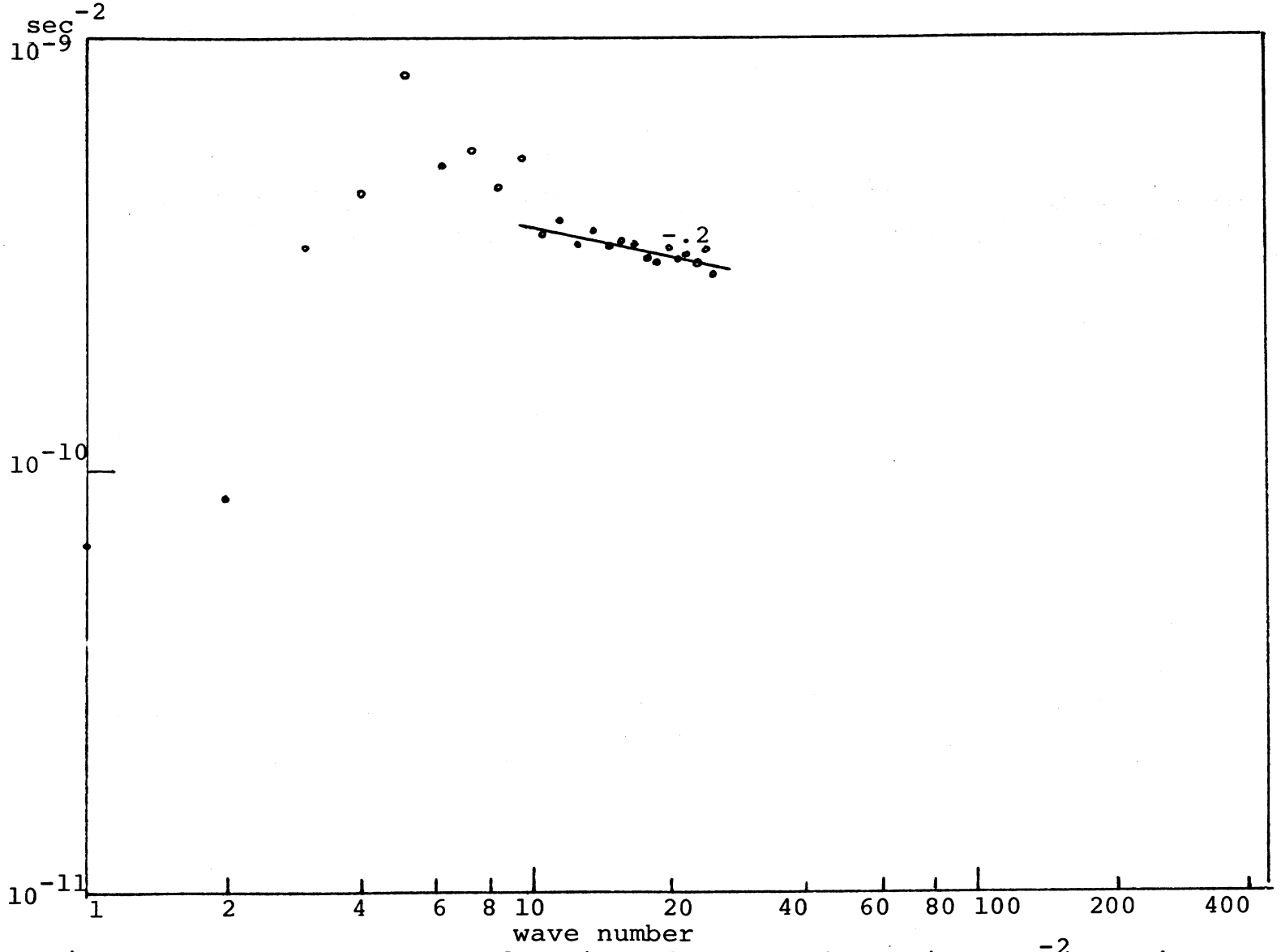

Figure 3.8: Enstrophy as a function of wave number.Units:sec^{-2}.Exp.4.

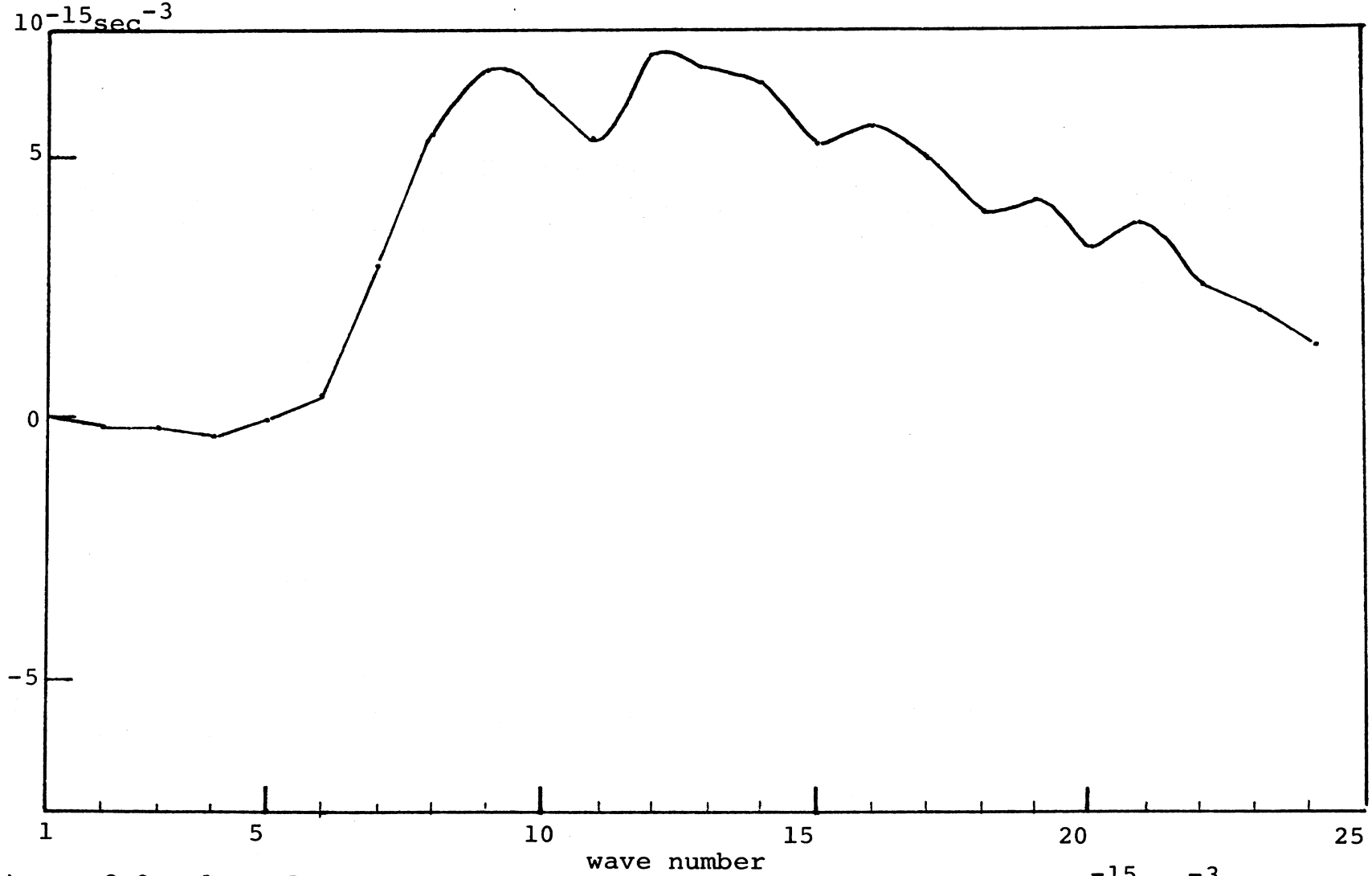

Figure 3.9: Flux of enstrophy as a function of wave number. Units:$10^{-15}sec^{-3}$.Exp.4.

It is of interest to compare the energetics of experiment 1 with those of experiment 4. Figures 3.10 and 3.11 depict the non-linear conversions of available potential energy and kinetic energy respectively for experiment 1. Figure 3.12 depicts the conversion from available to kinetic energy. The generation of available potential energy is in wave number 8. While potential energy is cascaded both up and down the spectrum the predominant gain is by the smaller scales ($\kappa>8$). It is interesting to note that there is a small loss of available potential energy, due to non-linear cascades, in waves 1 to 5. This loss is compensated in part by a conversion of kinetic energy to available potential energy in these same waves (Figure 3.12). The non-linear cascade of kinetic energy is predominantly from wave number 8 to the larger scales.

While both kinetic and potential energy are cascaded out of the potential energy source region, Figure 3.12 demonstrates that potential energy is converted to kinetic energy predominantly in this source region. This in in contrast to experiment 4 where the conversion is predominant in the range $3\leq\kappa\leq5$.

The non-linear enstrophy gain is shown in Figure 3.13. This figure demonstrates that the predominant enstrophy cascade is toward smaller scales.

Finally we show, in Figures 3.14, 3.15, and 3.16, the spectral distribution of kinetic energy, available potential energy, and enstrophy respectively. Apart from the sharp local

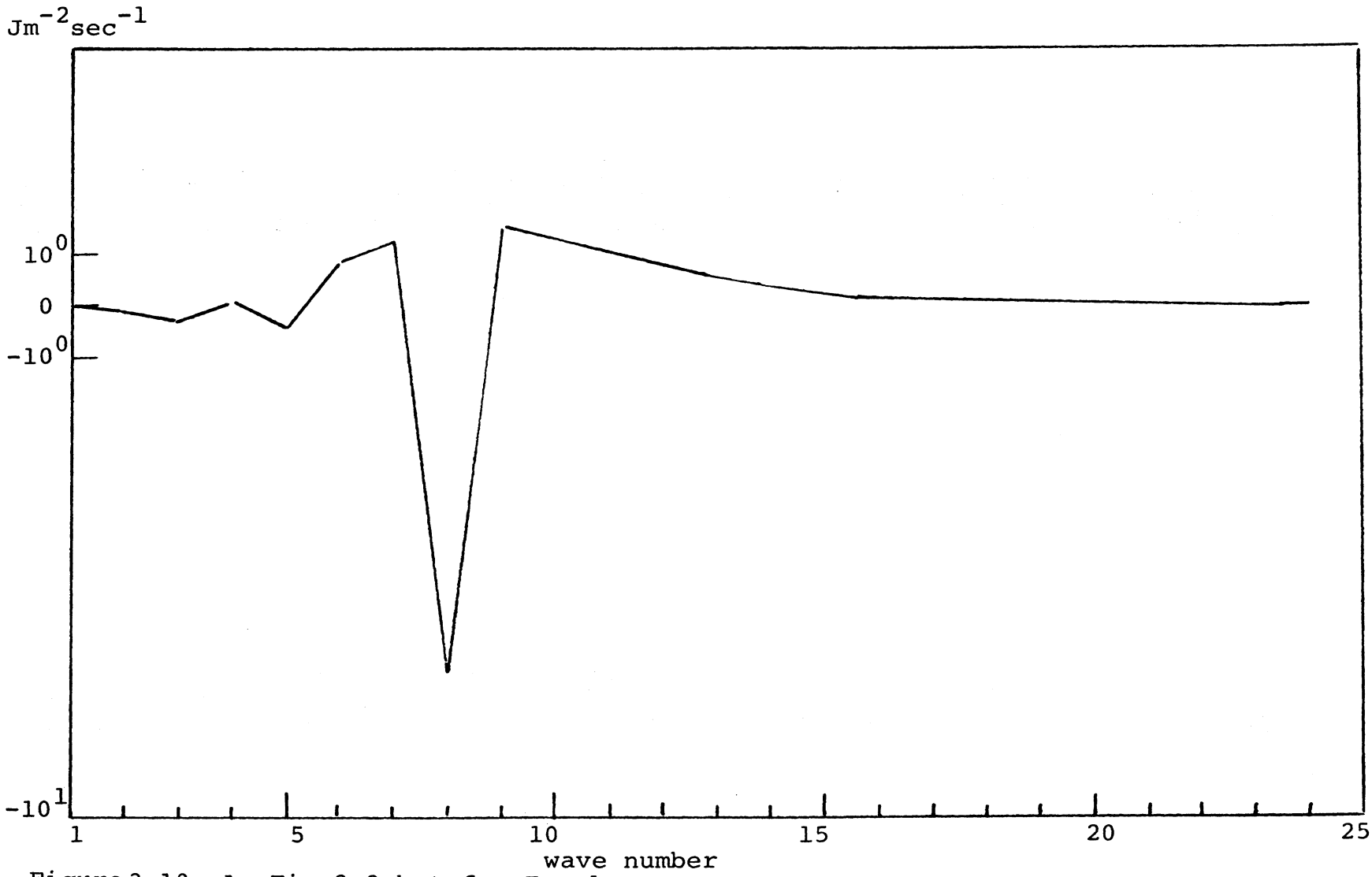

Figure 3.10: As Fig.3.3 but for Exp.1.

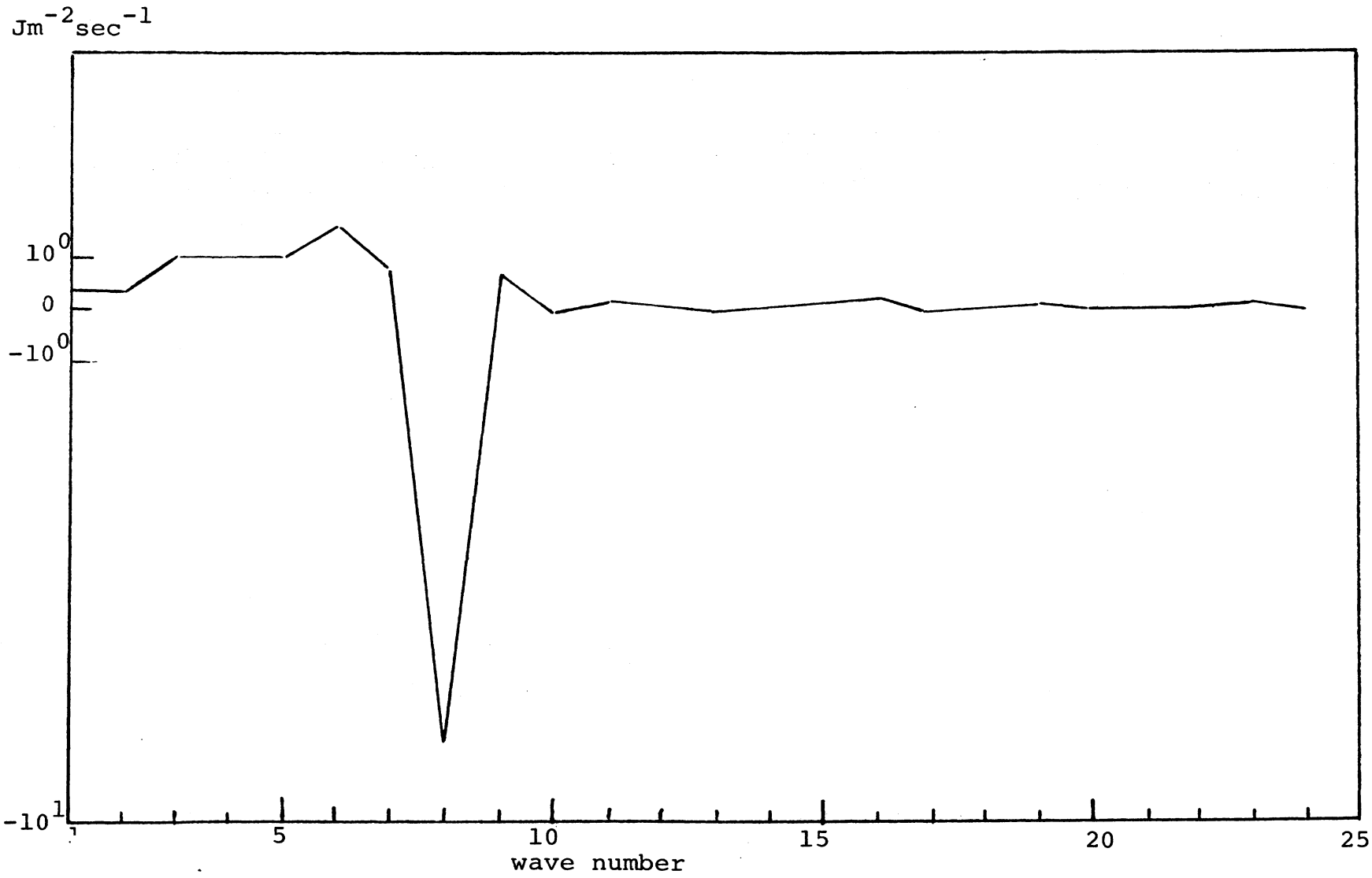

Figure 3.11: As Fig.3.4 but for Exp.1.

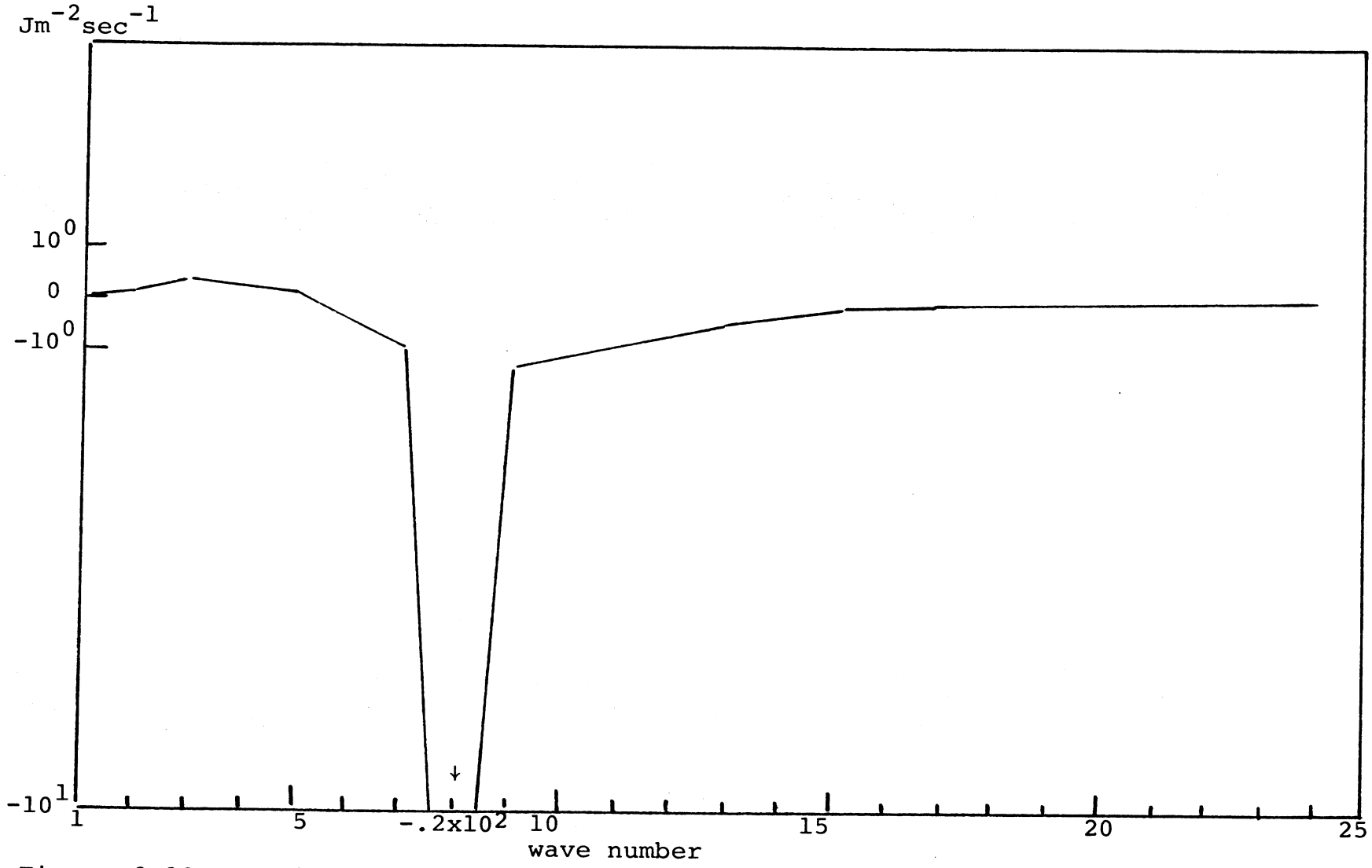

Figure 3.12: As Fig.3.5 but for Ex[illegible]

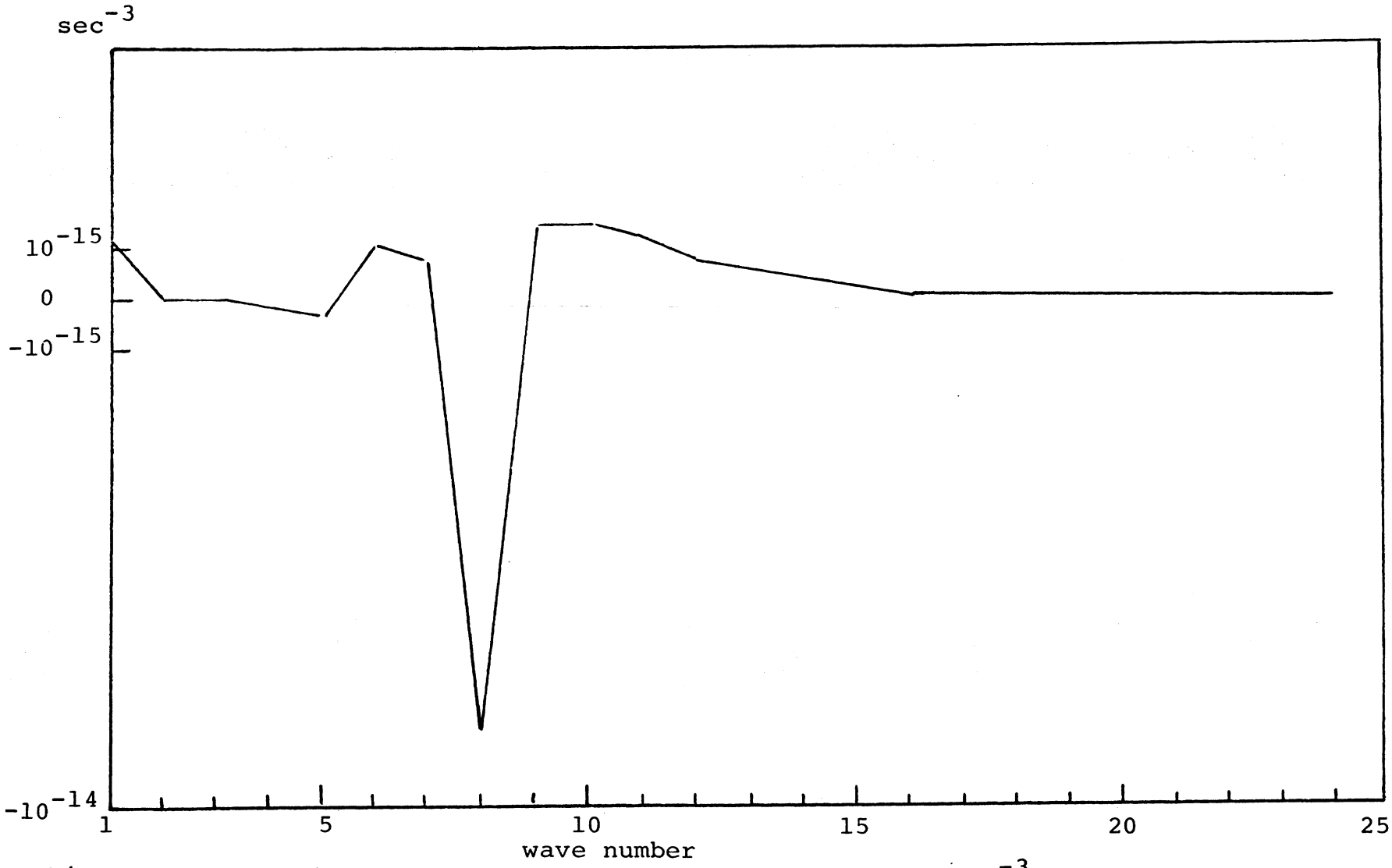

Figure 3.13: I(m/n,ℓ), nonlinear gain of enstrophy.Units:sec^{-3}.Exp.1.

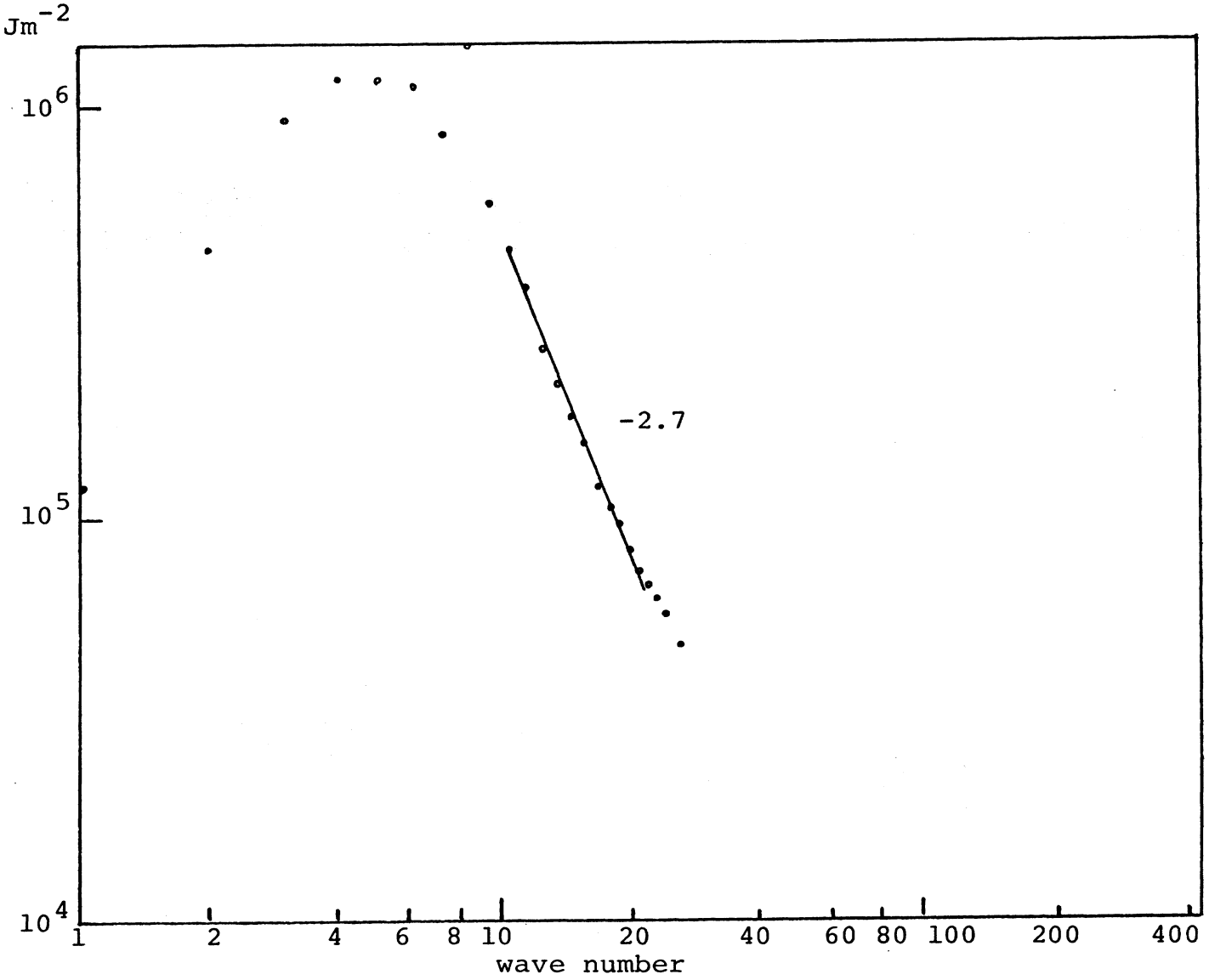

Figure 3.14: As Fig.3.6 but for Exp.1.

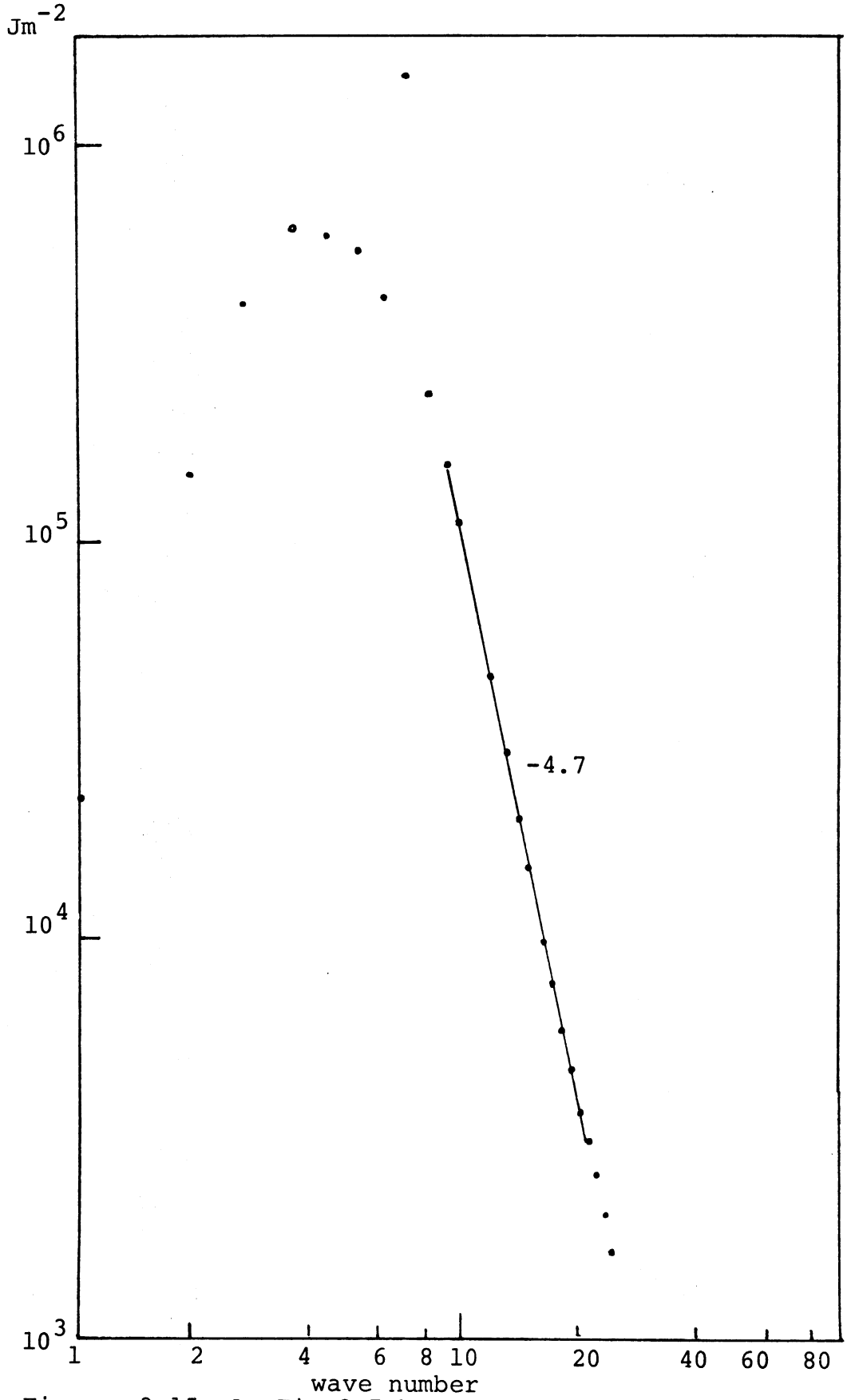

Figure 3.15: As Fig.3.7 but for Exp.1.

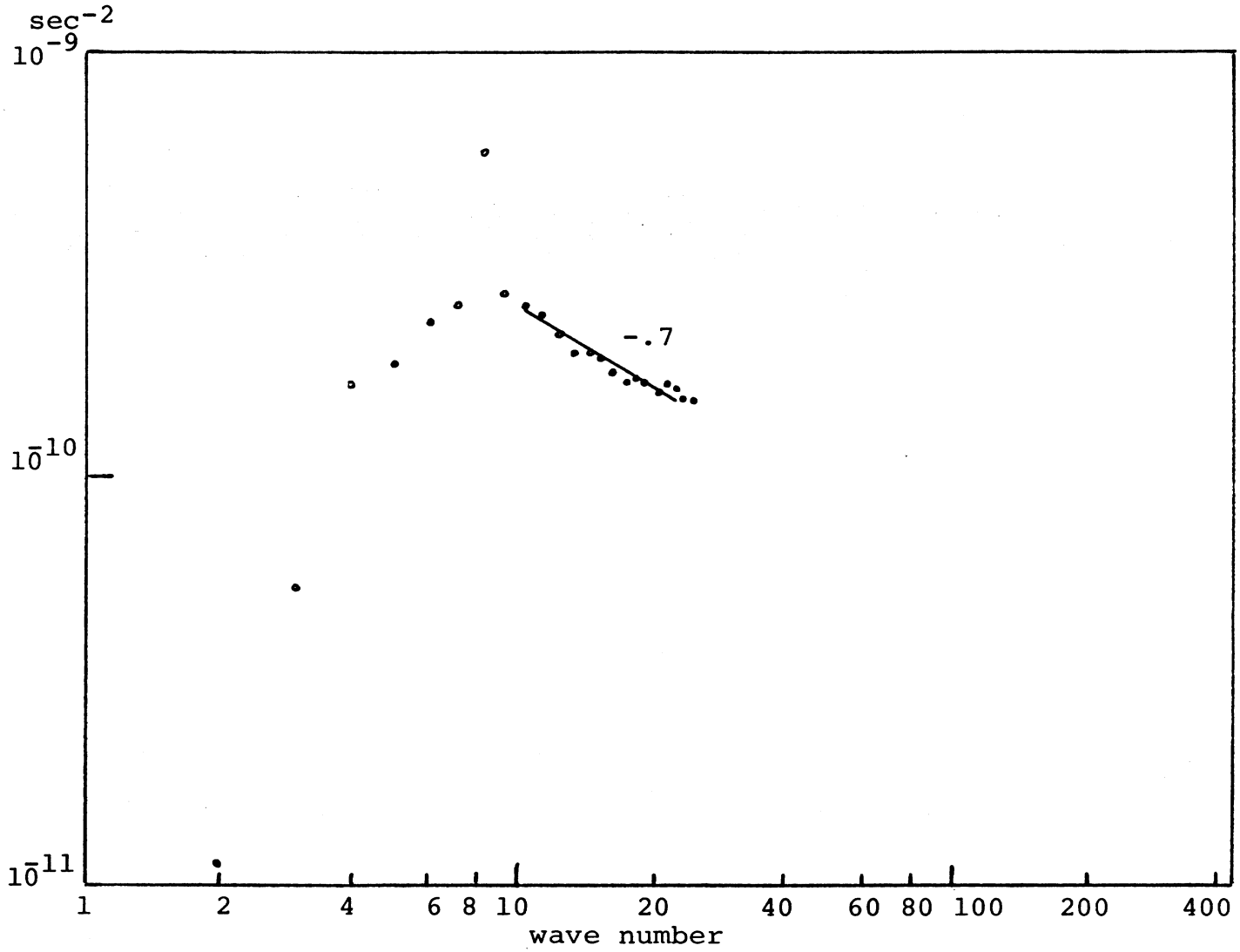

Figure 3.16: As Fig.3.8 but for Exp.1.

maximum at wave number 8 the energy maxima are at wave number 4. The slopes of -2.7 and -4.7 in the range $10<\kappa<20$ are in fair agreement with the -3 and -5 which may be deduced from the current quasi-geostrophic turbulence theories.

4. THE EFFECT OF VARYING FRICTIONAL PARAMETERS

We shall now proceed to a comparison of the results of experiments 2 and 3 with those of 1. Discussion of experiment 2 can be limited at the outset to the comment that the results differ only in minor respects from those of experiment 1. This is perhaps best illustrated by examining the energy and enstrophy spectra for this case. These are shown in Figures 4.1 through 4.3. It is apparent from these figures that the effect of modifying the boundary layer frictional coefficient is very minor in this case, especially as regards the structures of the spectra for high wave numbers ($\kappa>10$). This is in agreement with the conclusions reached in BW.

On the other hand the effect of introducing horizontal friction is quite pronounced, again in agreement with the conclusions of BW. The energy and enstrophy spectra for experiment 3 are shown in Figures 4.4 through 4.6. It is apparent not only that the slopes in the range $\kappa \geq 10$ are steeper but also that they deviate systematically from constant values, tending to steeper for the higher wave numbers.

This behaviour is also consistent with the theory presented in BW where it is shown from similarity arguments that the

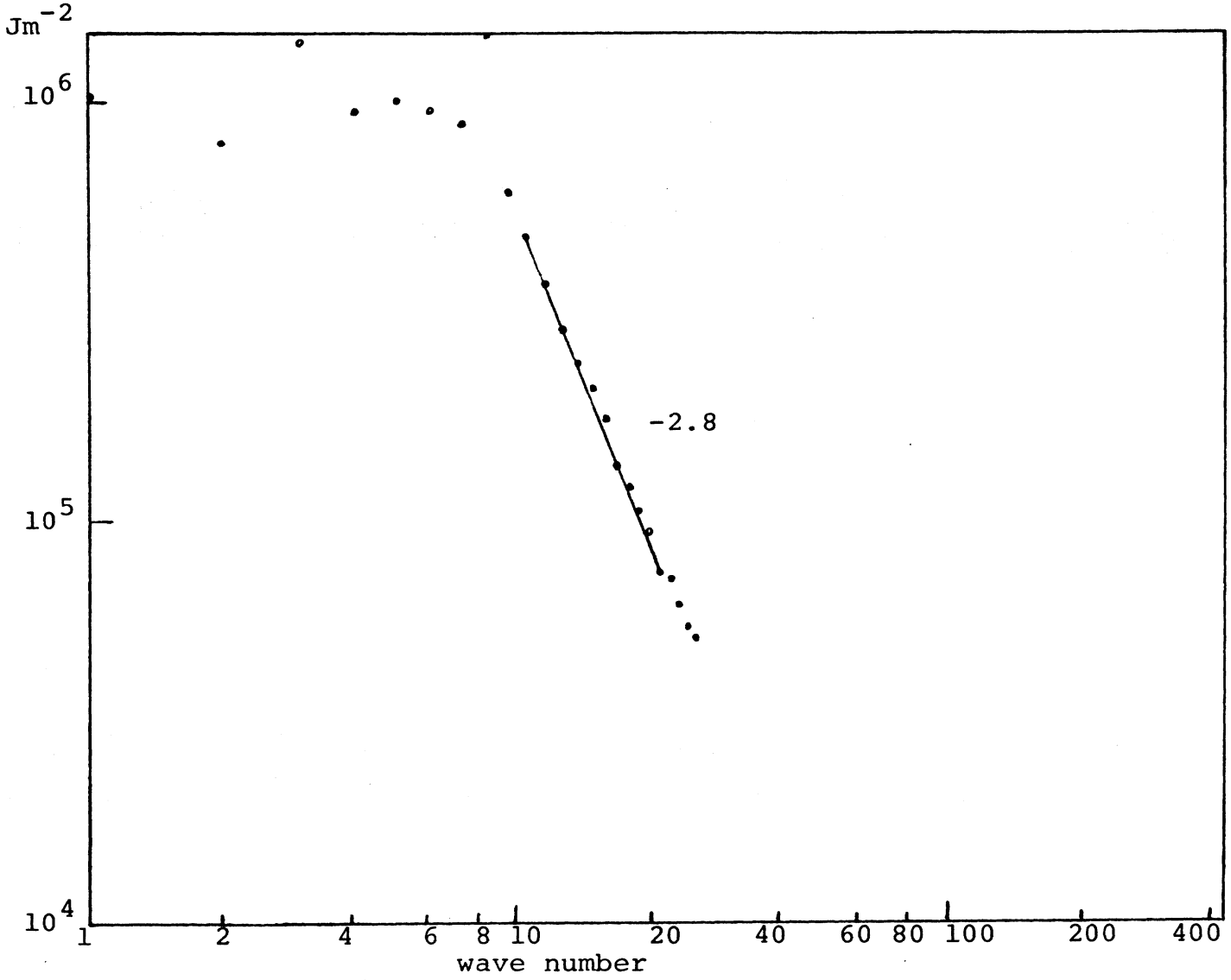

Figure 4.1: As Fig.3.6 but for Exp.2.

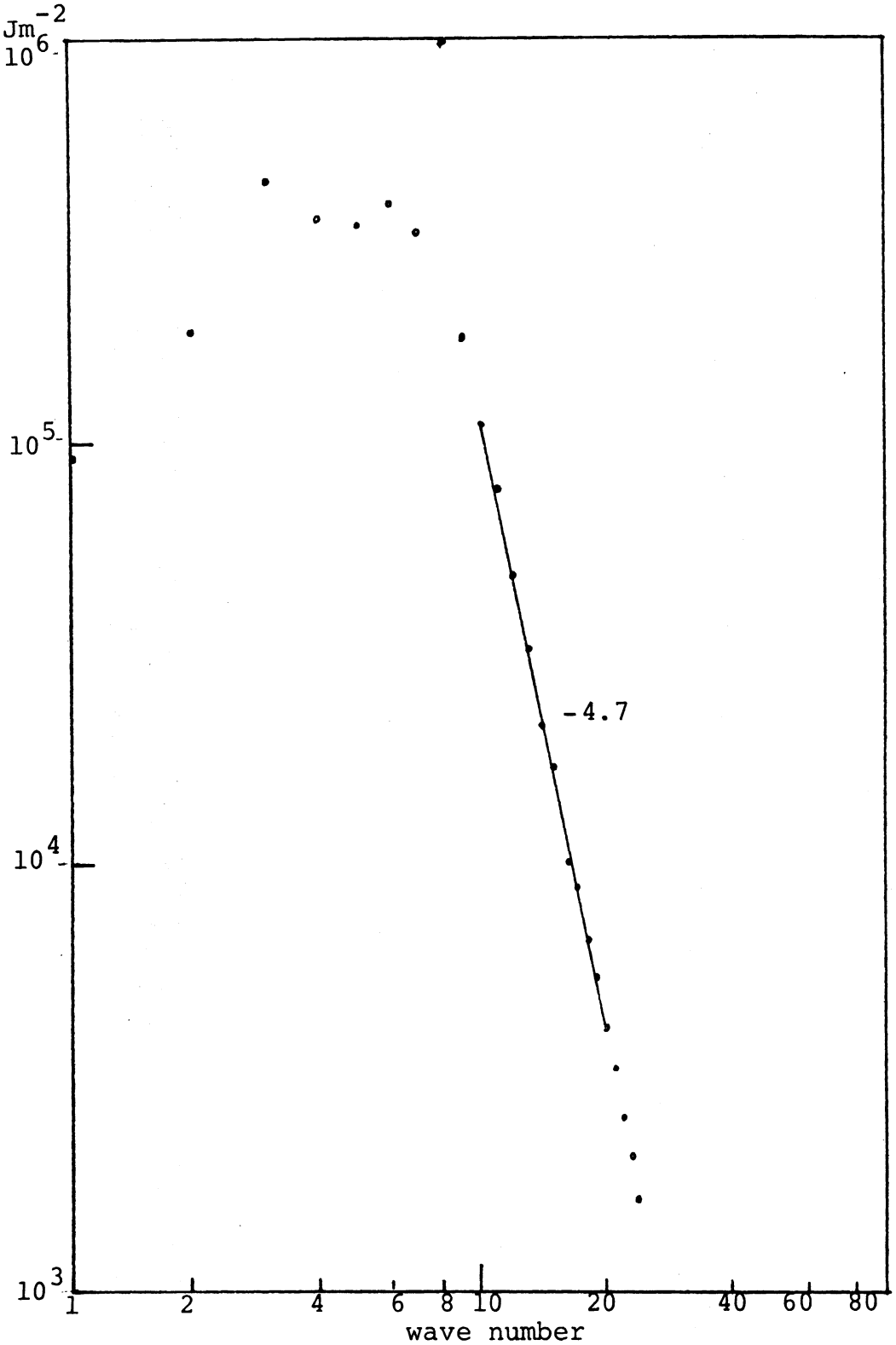

Figure 4.2: As Fig.3.7 but for Exp.2.

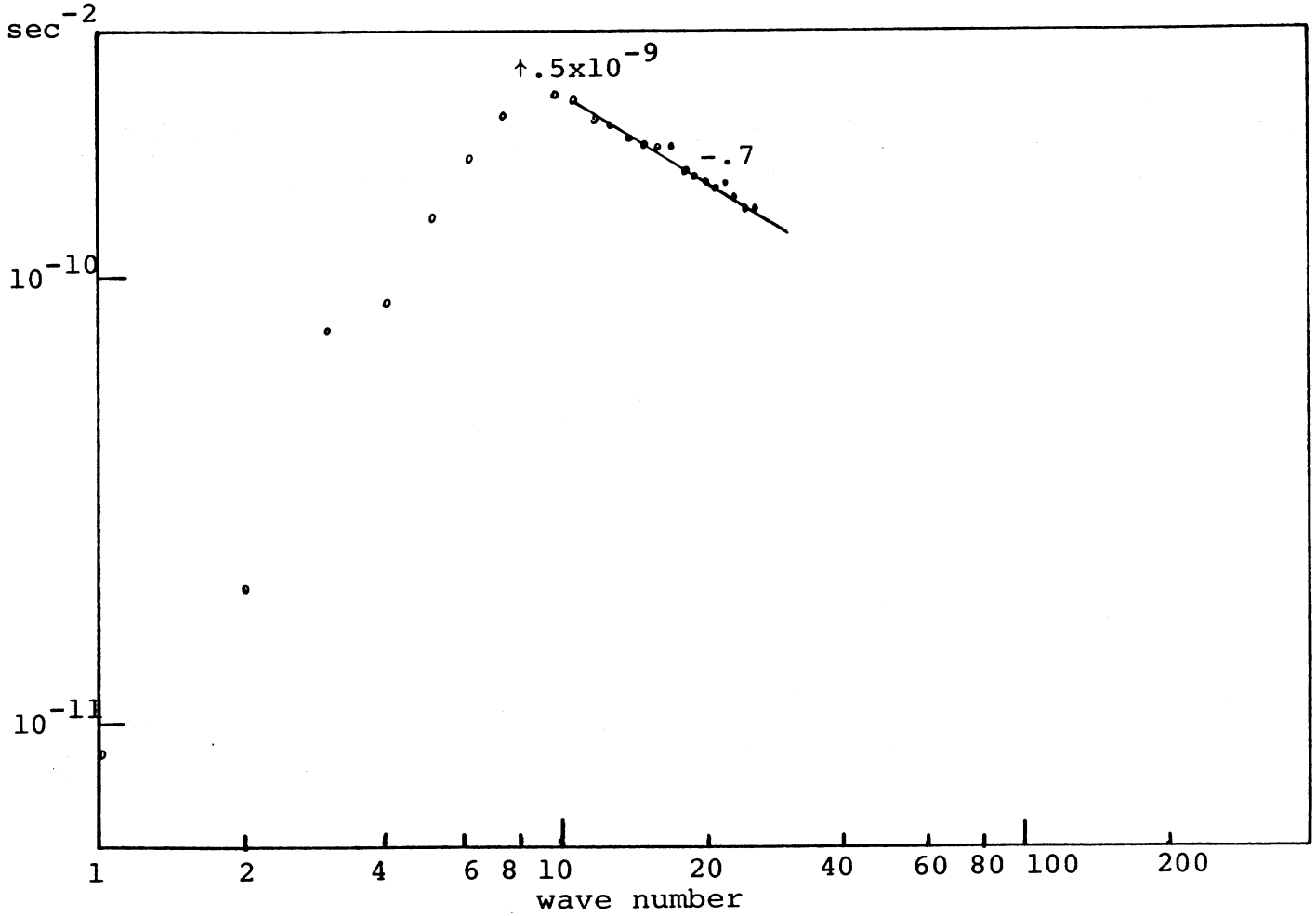

Figure 4.3: As Fig.3.8 but for Exp.2.

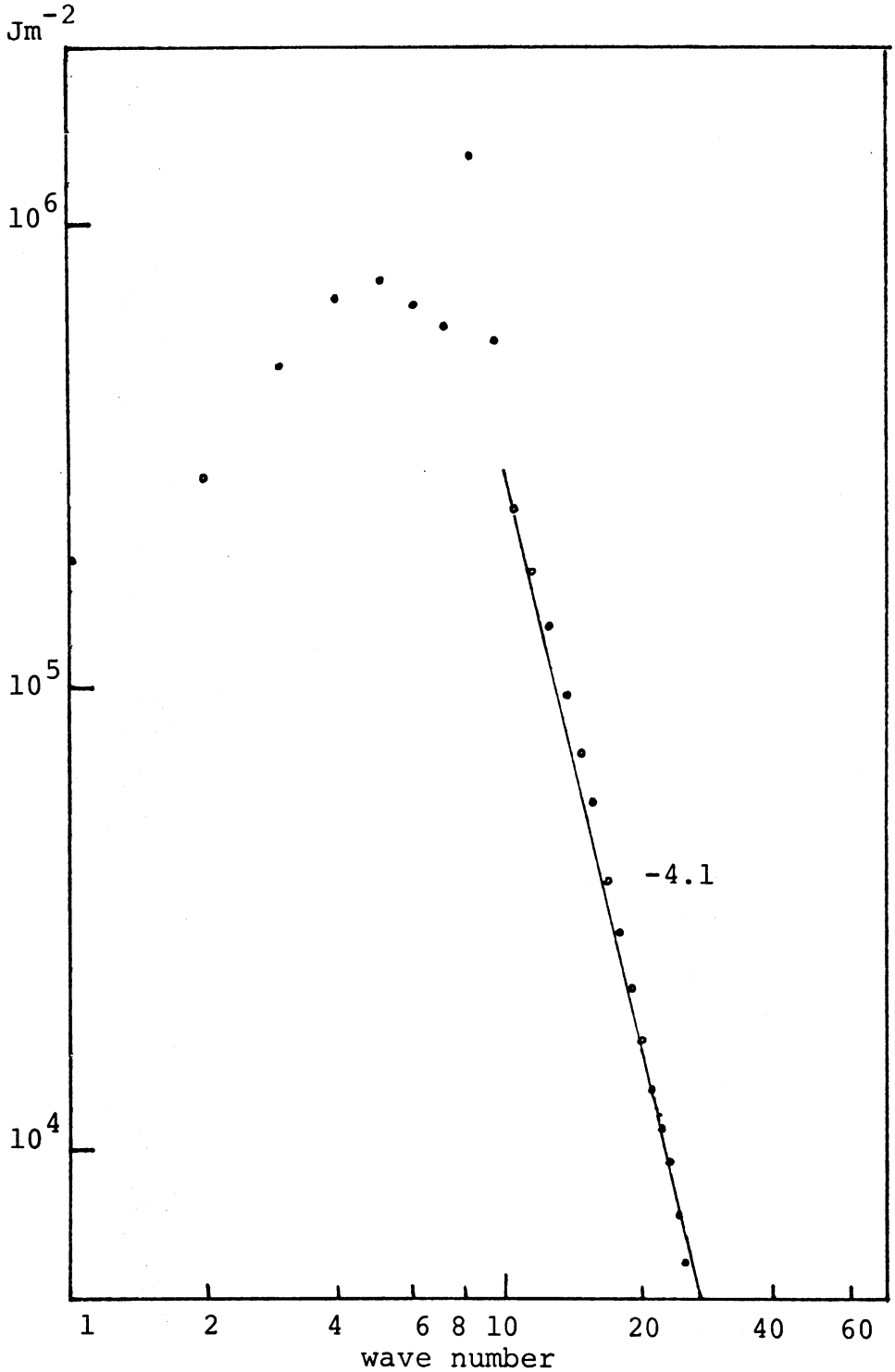

Figure 4.4: As Fig.3.6 but for Exp.3.

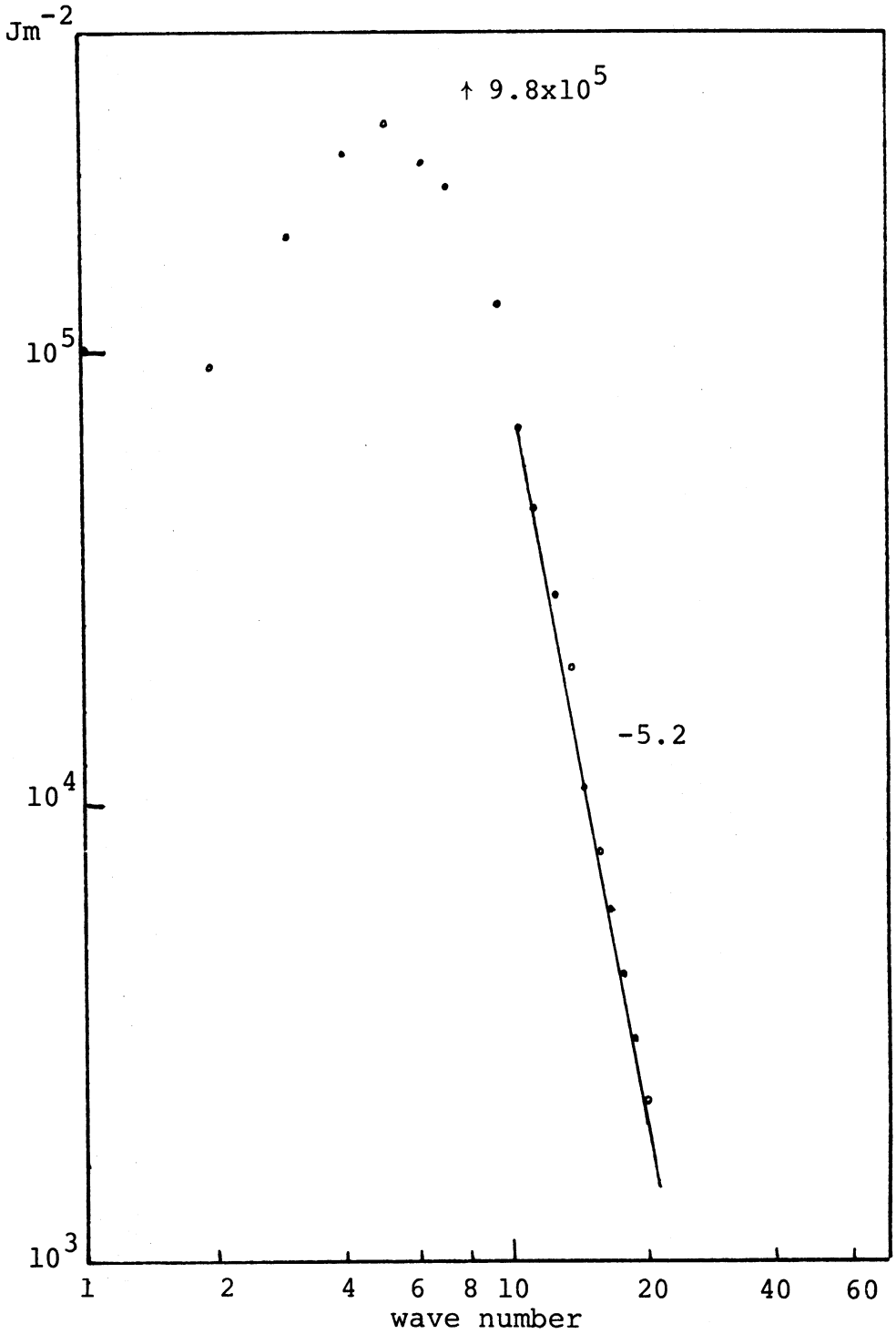

Figure 4.5: As Fig.3.7 but for Exp.3.

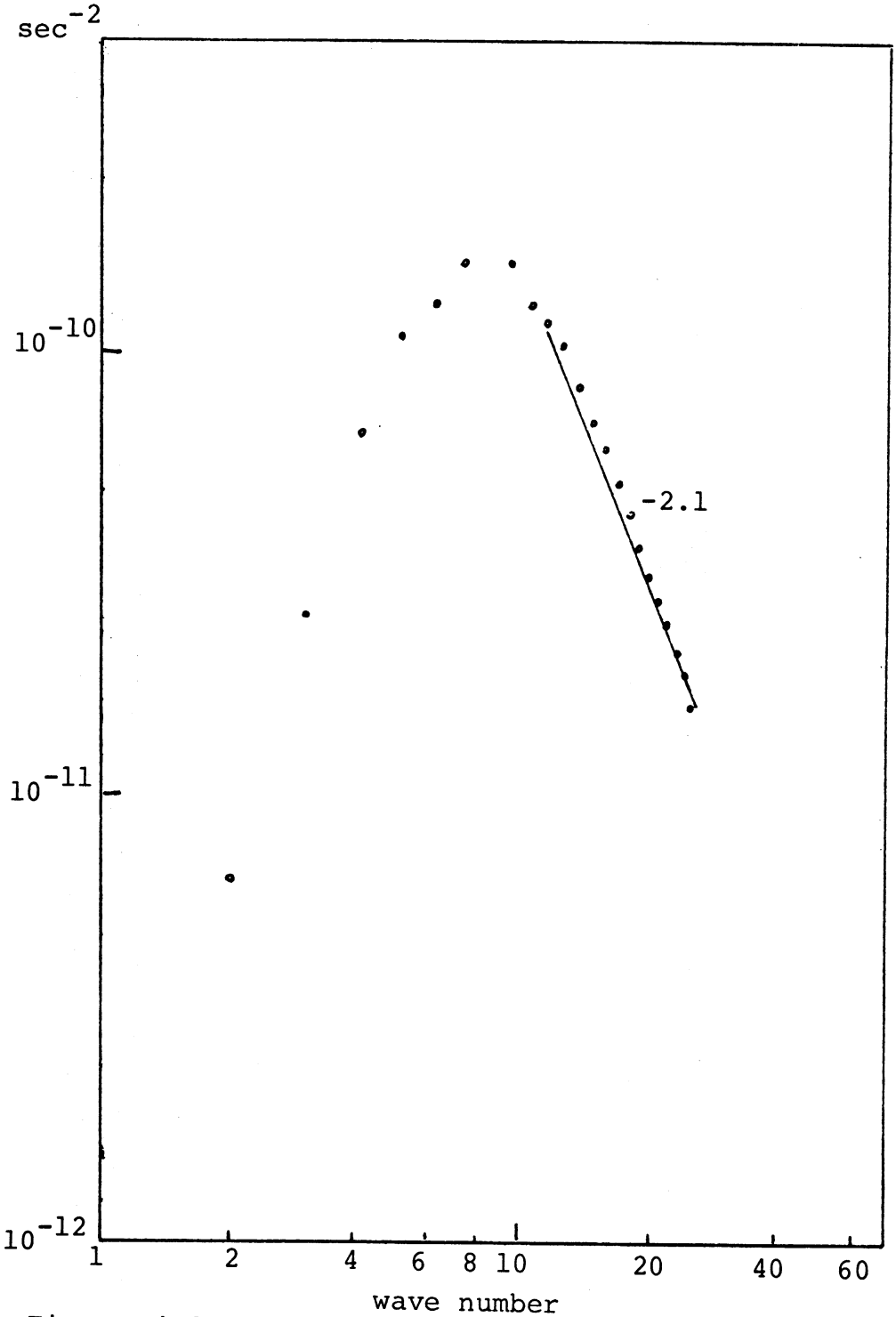

Figure 4.6: As Fig.3.8 but for Exp.3.

-3 power law for the kinetic energy spectrum in high wave numbers can be modified, when $\nu \neq 0$ to the following form:

$$K(\kappa) \propto \kappa^{-3} \exp\left[-\frac{\alpha}{\kappa_o^2}(\kappa^2 - \kappa_e^2)\right], \quad \kappa > \kappa_e \tag{4.1}$$

where

$$\kappa_o = \eta_e^{1/6} \nu^{-1/2}$$

and α is a dimensionless constant. Here η_e is the enstrophy cascade rate at $\kappa = \kappa_e$.

Where boundary layer friction is present in the model also 4.1 is modified to

$$K(\kappa) = \kappa^{-(3+\alpha s)} \exp\left[-\alpha \frac{\kappa^2 - \kappa_e^2}{\kappa_o^2}\right] \tag{4.2}$$

where $s = ka/\eta_e^{1/3}$, $a = 0.2$, and k is the boundary layer frictional coefficient. For experiment 3 $\alpha s \simeq 0.8$. Equation (4.2) explains the steepering of the spectrum for large values of $\kappa (\kappa >> \kappa_e)$.

5. A THEORETICAL DISCUSSION OF THE DISTRIBUTION OF ENERGY UNDER QUASI-STEADY CONDITIONS FOR EXPERIMENT 3

A characteristic feature of all the experiments which have been discussed is that the evolution of energy and potential enstrophy is such that, after an initial adjustment period, these quantities become quasi-steady. In order for this state to be maintained there must be an approximate balance between generation and dissipation of both energy and enstrophy. Some insight into the distribution of energy in wave number space in this situation

can be obtained by examining explicitly the circumstance in which there is an exact balance between generation and dissipation of energy and potential enstrophy. We shall confine attention to the role of lateral diffusion in maintaining this balance.

We define total potential enstrophy as follows:

$$\zeta^2_p = \frac{1}{2S}\int_s (q_1^2 + q_3^2)dA \tag{5.1}$$

where S is the total horizontal area of the model and dA is an increment of area. Now, taking $\partial\zeta_p^2/\partial t = 0$ we may easily show from equations 2.1 and 2.2 that the following must be true:

$$-\frac{1}{2S}\int_s (q_1 - q_3)HdA + \frac{\nu}{2S}\int_s [q_1\nabla^2 q_1 + q_3\nabla^2 q_3]dA = 0 \tag{5.2}$$

Similarly we define the total energy as the sum of available potential energy and kinetic energy as follows:

$$E = K + A = \frac{1}{2S}\int_s [(\nabla\psi_1)^2 + (\nabla\psi_3)^2 + \lambda^2(\psi_1 - \psi_3)^2]dA \tag{5.3}$$

If this quantity is also steady then it also follows from 2.1 and 2.3 that

$$-\frac{\nu}{S}\int_s [(\nabla^2\psi_1)^2 + (\nabla^2\psi_3)^2 + \lambda^2\nabla T\cdot\nabla T]dA + \frac{1}{S}\int_s HTdA = 0 \tag{5.4}$$

where $T = \psi_1 - \psi_3$.

We shall transform 5.3 and 5.4 into the wave number domain by defining the Fourier transforms of ψ_1 and ψ_3 to be given by

$$\psi_j = \sum_{m=-M}^{M} \sum_{n=-N}^{N} A_{j,m,n}\, e^{iJ(mx+ny)}, \qquad j = 1,3 \tag{5.5}$$

$$A_{j,-m,-n} = A^*_{j,m,n} \tag{5.6}$$

where $J = 2\pi/L$ and $L = 64\Delta x$. M and N can not exceed 32 in this case.

The following definitions will also be useful:

$$K_{m,n} = \frac{J^2}{2} \sum_{j=1,3} (m^2 + n^2)\, |A_{j,m,n}|^2 \tag{5.7}$$

$$B_{m,n} = A_{1,m,n} - A_{3,m,n} \tag{5.8}$$

$$P_{m,n} = \frac{\lambda^2}{2} \sum_{j=1,3} |B_{m,n}|^2 \tag{5.9}$$

$$K_\kappa = \sum_m \sum_n K_{m,n}; \qquad m^2 + n^2 = \kappa^2 \tag{5.10}$$

$$P_\kappa = \sum_m \sum_n P_{m,n}; \qquad m^2 + n^2 = \kappa^2 \tag{5.11}$$

We specify the heating function H to be made of a single Fourier component whose (integral) wave number is m, i.e.

$$H = \sum_\ell \sum_p H_{\ell,p}\, e^{iJ(\ell x + py)}, \qquad H_{-\ell,-p} = H^*_{\ell,p} \tag{5.12}$$

This expression for H, where used in 5.2 and 5.4 leads to the following

$$\sum_\kappa \left\{ \kappa^4 K_\kappa + \left(\frac{2\lambda^2}{J^2} + 2\kappa^4 \right) P_\kappa \right\} = \left(m^2 + \frac{2\lambda^2}{J^2} \right) \frac{|B_m H_m|}{2J^2 \nu} \tag{5.13}$$

$$\sum_{\kappa} \left\{ \kappa^2 K_\kappa + \kappa^2 P_\kappa \right\} = \frac{1}{2J^2\nu} |B_m H_m| \tag{5.14}$$

where

$$|B_m H_m| = \sum_{\ell} \sum_{p} (B_{\ell,p} H^*_{\ell,p} + B^*_{\ell,p} H_{\ell,p}), \qquad \ell^2 + p^2 = m^2 \tag{5.15}$$

Before proceeding further we may note that 5.13 provides some immediate information on the behaviour of K_κ. Since the right side of 5.13 is finite the sum on the left side must be also. If we ignore for the moment the practical requirement that κ must be bounded and assume that all integral values are permissible then it is obvious that, for large κ, K_κ must decrease more rapidly than κ^{-4}. (Note that, for large κ, $P_\kappa \sim \kappa^{-2} K_\kappa$). This requirement explains, in part at least, the steepening of the energy spectrum in the high wave number range which was observed in experiment 3.

In order to put 5.13 and 5.14 into more convenient form we define the following quantities:

$$K = \sum_{\kappa} K_\kappa \; ; \qquad P = \sum_{\kappa} P_\kappa \tag{5.16}$$

$$n_\kappa^{\,2} = (\sum_{\kappa} \kappa^2 K_\kappa)/K; \qquad n_\kappa^{\,4} = (\sum_{\kappa} \kappa^4 K_\kappa)/K \tag{5.17}$$

$$n_p^{\,2} = (\sum_{\kappa} \kappa^2 P_\kappa)/P; \qquad n_p^{\,4} = (\sum_{\kappa} \kappa^4 P_\kappa)/P \tag{5.18}$$

$$s^2 = 2\lambda^2/J^2 \tag{5.19}$$

Using these definitions it is easily shown, from 5.13 and 5.14, that

$$\frac{P}{K} = \frac{n_K^4 - n_K^2(s^2 + m^2)}{n_p^2 m^2 - 2n_p^4} \tag{5.20}$$

This result can, in turn, be used to show that

$$\sum_K [s^2\kappa^2 K_K - \kappa^4 P_K] = \sum_K [\kappa^4 - m^2\kappa^2](P_K + K_K) \tag{5.21}$$

A slight rearrangement of terms leads to a useful inequality:

$$\sum_K (2\kappa^4 - m^2\kappa^2)(P_K + K_K) = \sum_K (s^2\kappa^2 + \kappa^4)K_K > 0 \tag{5.22}$$

Consequently most of the contribution to the sum on the left hand side of (5.22) must come from scales which are smaller than that defines by $\kappa^2 = m^2/2$.

If it should happen that the right side of 5.21 is also positive (i.e. most of the contribution comes from scales which are smaller than the generation scale) then

$$s^2 \sum_K \kappa^2 K_K > \sum_K \kappa^4 P_K \tag{5.23}$$

This inequality appears to be satisfied for experiment 3. In that case $s^2 \simeq 75$ so that $s^2\kappa^2 > \kappa^4$ for $\kappa < 8$. Moreover $K_K > P_K$ everywhere.

The experiments also show that, typically, potential energy is cascaded to smaller scales while kinetic energy is cascaded to larger scales. Now the denominator of 5.20 will be negative if there is a sufficient potential energy in the small scales so that

$$\sum_{K} (\kappa^2 m^2 - 2\kappa^4) P_K < 0 \qquad (5.24)$$

When this is the case the numerator of 5.20 must also be negative and this implies that

$$\sum_{K} [\kappa^4 - (s^2 + m^2)\kappa^2] K_K < 0 \qquad (5.25)$$

or, that most of the kinetic energy must be contained in scales which are larger than that defined by $k^2 = s^2 + m^2$.

The above inequalities are most likely to be satisfied when m is small. In particular 5.23, 5.24 and 5.25 are all satisfied when m=1. All of the experiments share the feature that K>P when equilibrium is established. This is consistent with the fact that available potential energy is cascaded to smaller scales while kinetic energy is cascaded to larger scales.

The truth of the preceding statement for experiment 3 is illustrated by Figures 4.4 and 4.5 and by Figure 5.1 which depicts the time evolution of energy for this case. It is interesting to examine also the non-linear energy conversions for this experiment. These are shown in Figures 5.2 and 5.3. It is apparent from these figures that kinetic energy is cascaded predominantly to lower wave numbers while potential energy is cascaded to higher wave numbers.

6. CONCLUDING REMARKS

It is useful at this stage to summarize the salient features of the various experiments discussed in this report. To begin with we examined experiment 4 which differed from the others

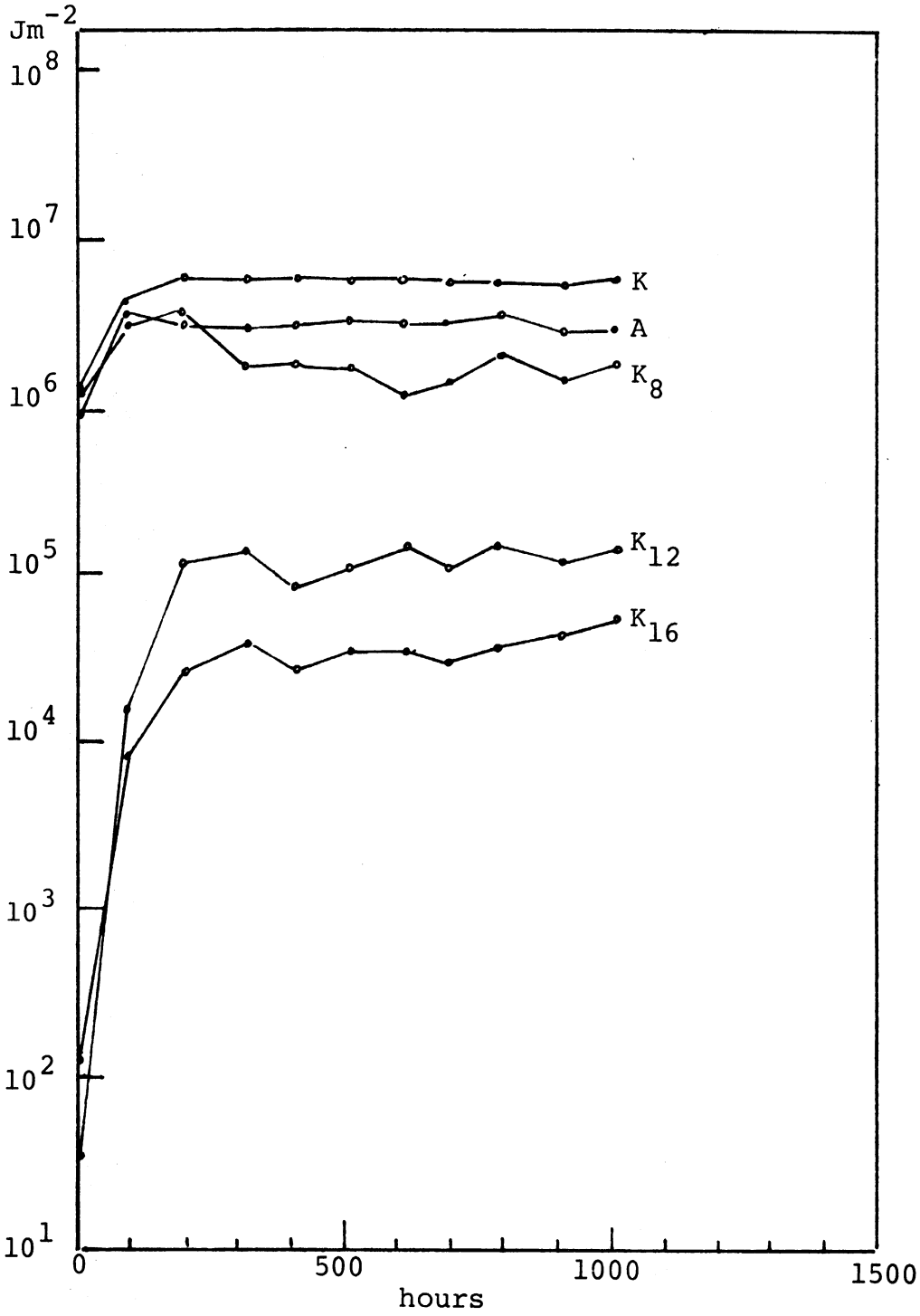

Figure 5.1: As Fig.3.2 but for Exp.3.

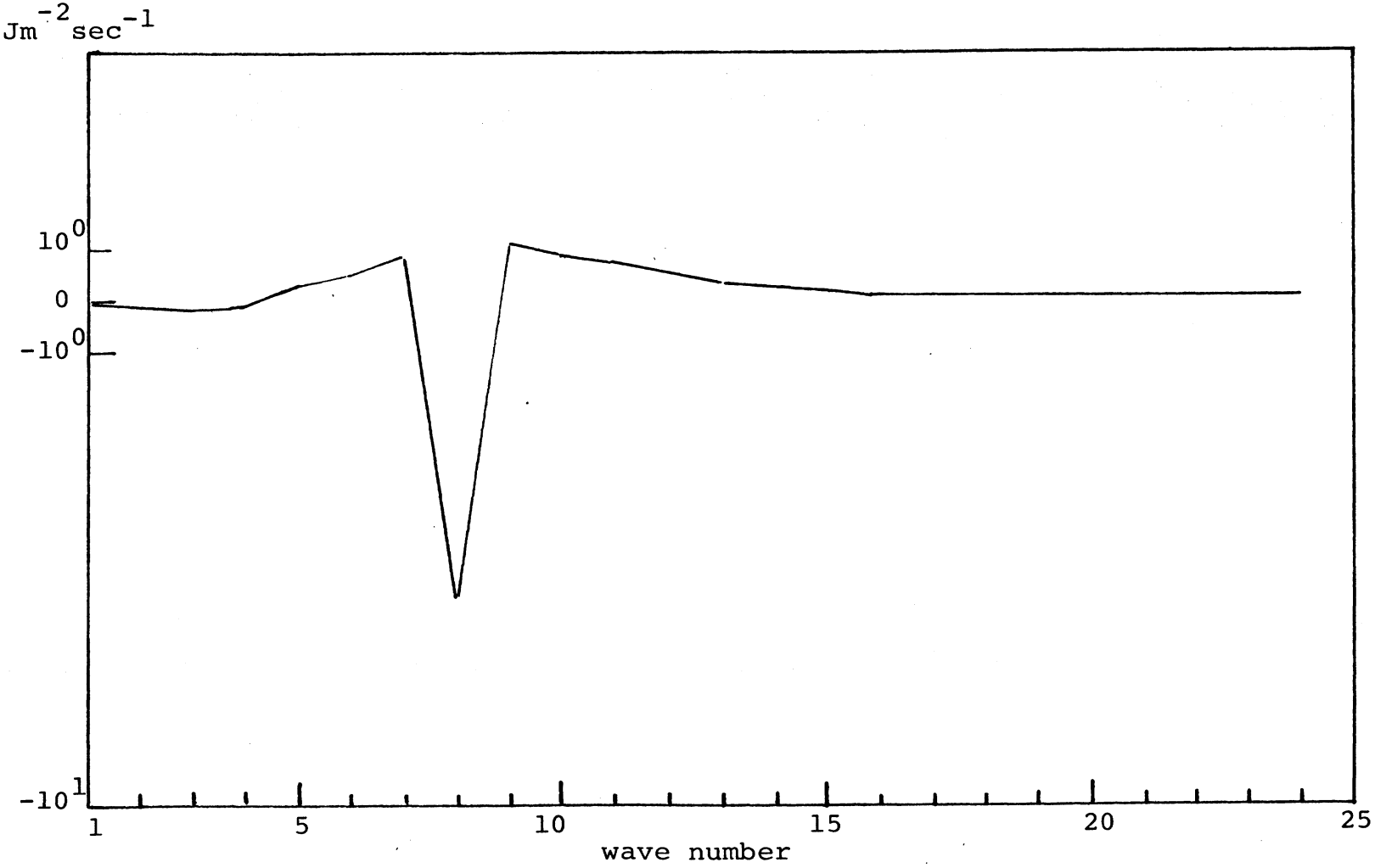

Figure 5.2: As Fig.3.3 but for Exp.3.

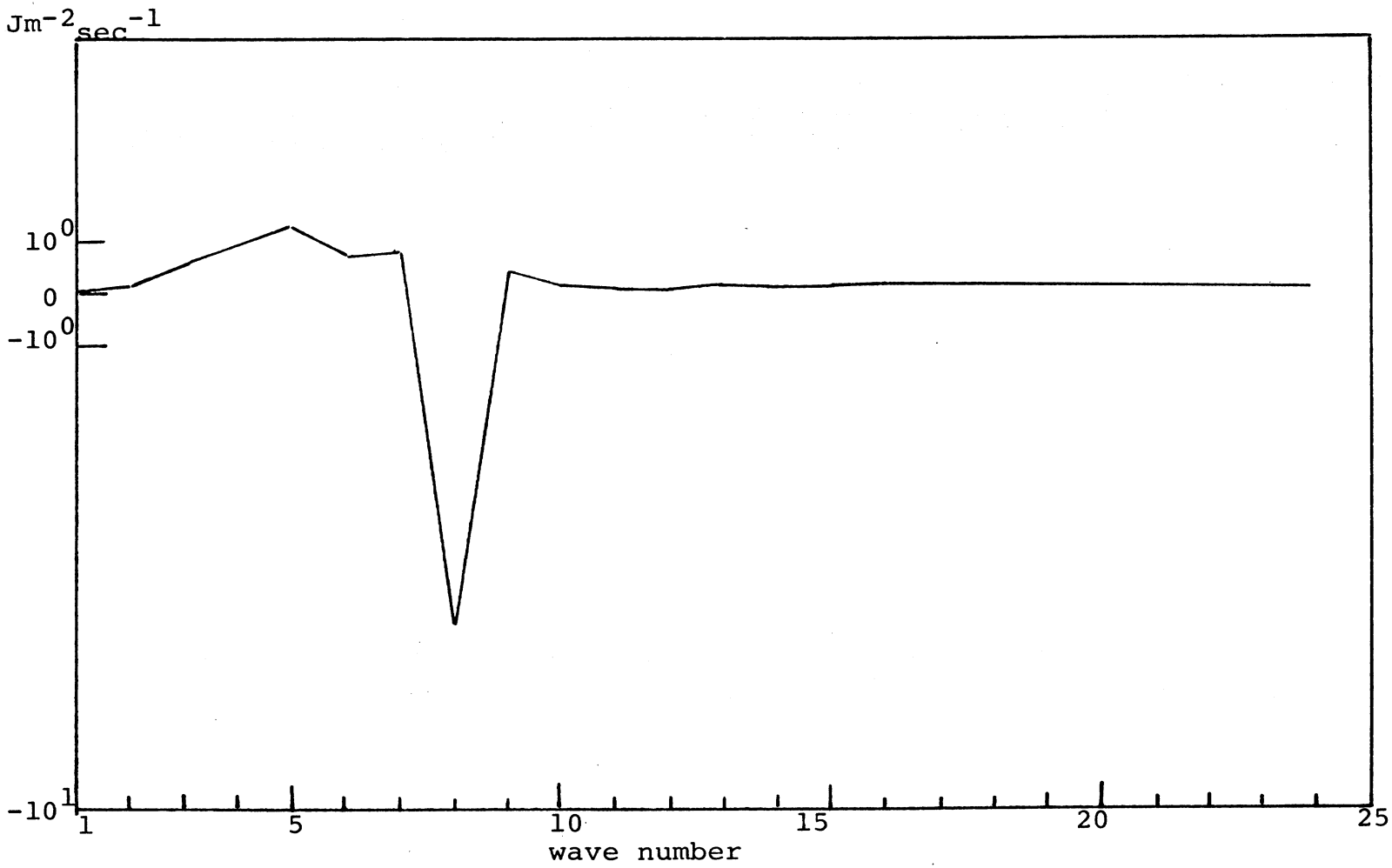

Figure 5.3: As Fig.3.4 but for Exp.3.

in that the forcing scale was that corresponding to $\kappa=1$, the largest permitted scale.

There were several distinctive features in the results of experiment 4. First of all the total amount of energy generated was larger than that in the other experiments. Moreover, although available potential energy was dominant in the early stages of the time evolution, kinetic energy eventually dominated. Another interesting feature was that under near equilibrium conditions the predominant conversions of available potential energy to kinetic energy were in the wave number range $3<\kappa<5$. In this respect the model behaved in a manner reminiscent of the channel model discussed in BW. By analogy with that study, the range $3<\kappa<5$ would appear to be the baroclinically active range for experiment 4. It is also interesting to note that kinetic energy is cascaded to larger scales from scales in the range $7<\kappa<9$. This behaviour also resembles, qualitatively, that of the channel model in BW.

The remaining experiments were designed to test the effect of varying frictional parameters. The forcing scale for these experiments were chosen to correspond to wave number 8. The energy generation was much less efficient in these experiments (i.e. as compared to experiment 4) and as a consequence the equilibrium state was reached much more quickly (typically in 100-300 time steps as compared to approximately 800 for experiment 4). This lack of efficiency may, in part, be due to the possibility that $\kappa=8$ is a scale which is smaller than the baroclinically active scale. Consequently, the available potential energy to kinetic energy

conversions are less effective both in the generation region near $\kappa=8$ and in the region $3<\kappa<5$. This latter region is inhibited because potential energy is cascaded mainly to scales which are smaller than the generation scale.

The results of experiments 1 and 2 were very similar. However, these results differ significantly from those for experiment 3. Perhaps the most marked difference was in the behaviour of the kinetic energy spectra for high wave numbers. In experiment 2 this spectrum followed, fairly closely, a -3 power law. In contrast experiment 3, which has a horizontal frictional mechanism, showed a pronounced steepering of the spectrum in the high wave numbers. In fact the spectrum deviates systematically from a power law behaviour in this range of wave numbers.

7. ACKNOWLEDGMENTS

The research leading to this paper has been supported in part by the National Science Foundation under Grant GA-16166. The numerical experiments were made by the computer operated by the National Center for Atmospheric Research which is supported by the National Science Foundation. The authors would furthermore like to thank Dr. Norman McFarlane and Miss Maria R. Perez-Discerni who gave a considerable contribution in the preparation of the manuscript. As in the first study Dr. James Pfaendtner was in charge of the programming and the numerical aspects of the calculations.

REFERENCES

Barros, V.R. and A. Wiin-Nielsen, 1974: On Quasi-Geostrophic Turbulence: A Numerical Experiment. J. Atmos. Sci., 31, 609-621.

Merilees, P.E. and T. Warn, 1972: The resolution implications of geostrophics turbulence. J. Atmos. Sci., 29, 900-991.

Steinberg, H.L., 1971: On power laws and non-linear cascades in large-scale atmospheric flows. Tech. Rept. 002630-T, The University of Michigan, Ann Arbor, 143 pp.

Steinberg, H.L., 1973: Numerical simulation of quasi-geostrophic turbulence, Tellus, 25, 233-246.